Design of the Adjustable Hydraulic Structure for Sea Lamprey Blockage Operations

August, 2016

Prepared by RiverRestoration.org[1]

Copy prepared for GLFT Grant 2015.1604

[1] Corresponding authors: Michael Scurlock – Hydraulic Engineer; michael.scurlock@riverrestoration.org; Jason Carey – Principal Engineer; jason.carey@riverrestoration.org; Scott Prins – Hydraulic Engineer; scott.prins@riverrestoration.org;. (970) 947-9568.

CONTENTS

1. INTRODUCTION

The sea lamprey (*Petromyzon marinus*) is an invasive, parasitic fish to the Great Lakes Fishery that has been culpable of mass detriment to populations of native species such as lake trout (*Salvelinus namaycush*), steelhead (*Oncorhynchus mykiss*), whitefish (*Coregonus clupeiformis*), and chub (*Coesius plumbeus*), resulting in significant economic decline (GLFC, 2000). Sea lampreys reside primarily in the Great Lakes where they prey on native species through oral disk attachment and blood leeching. Migration upstream into the tributaries of the Great Lakes Fishery occurs during spawning periods of late spring and early summer. Efforts to prevent sea lampreys from accessing spawning habitat have included the construction of instream, physical barriers which operate to block passage while allowing for jumping fish species mobility. Limiting access to upstream spawning habitat decreases lamprey production, reduces the need for lampricide treatments, and decreases economic expenditures. Approximately 50 barriers have been constructed, and 20 additional dams modified, for the sole intent of sea lamprey blockage (GLFC, 2016).

The Grand River at Grand Rapids, MI contains a grade-control structure, locally known as the 6th Street Dam, which lies approximately 40 miles upstream of Lake Michigan. The 6th Street Dam, depicted in Figure 1, is considered an effective sea lamprey barrier to upstream spawning areas and is the first structure which effectively impedes upstream passage. There are an estimated 1,268,891 m^2 of preferred larval habitat and 6,462,268 m^2 of acceptable larval habitat in the Grand River watershed upstream of the 6th Street Dam (Hanschue *et al*., 2011). Spawning habitat areas would be activated in the absence of the physical barrier existing within the channel. The current grade-control structure is nearing the end of its expected life capacity and will require maintenance and repair the near future in order to remain effective.

The Grand Rapids Revitalization project has been proposed to restore regionally rare rapids habitat to the Grand River at Grand Rapids, MI. Figure 2 illustrates a schematic of the proposed conditions at the finalization of the project. The existing 6th Street Dam location is illustrated in subsection R.280. As part of the project, the 6th Street Dam will be lowered and reconfigured to pass all fish species and activate unique upstream habitat which is currently inaccessible and submerged. Continued blockage of sea lamprey is a primary design constraint for the project and an upstream location for the construction of a new, dynamically operated adjustable hydraulic structure (AHS) has been proposed to serve specifically as a physical barrier for upstream sea lamprey passage while allowing jumping fish species to move freely. Optimization of the location of the AHS, and examination of the AHS to produce blockage hydraulics which meet literature recommendations and minimally meet the conditions at the 6th Street Dam, was examined in a feasibility report from RiverRestoration (2016a). The feasibility study indicated that the proposed AHS would properly function as a sea lamprey barrier under recommended operations and improve performance compared to the existing conditions.

The hydraulic design of the AHS to operate as a sea lamprey barrier expanded on findings from RiverRestoration (2016a) to create a functional structure under the range of design discharges. One-dimensional, two-dimensional, and three-dimensional hydraulic models were utilized to optimize the structural design to meet or achieve specific hydraulic blockage criteria as recommended from the literature. This report details the specific hydraulic design of the AHS, including targets, constraints, operational configurations, and resulting performance.

Figure 1. Existing 6th Street Dam

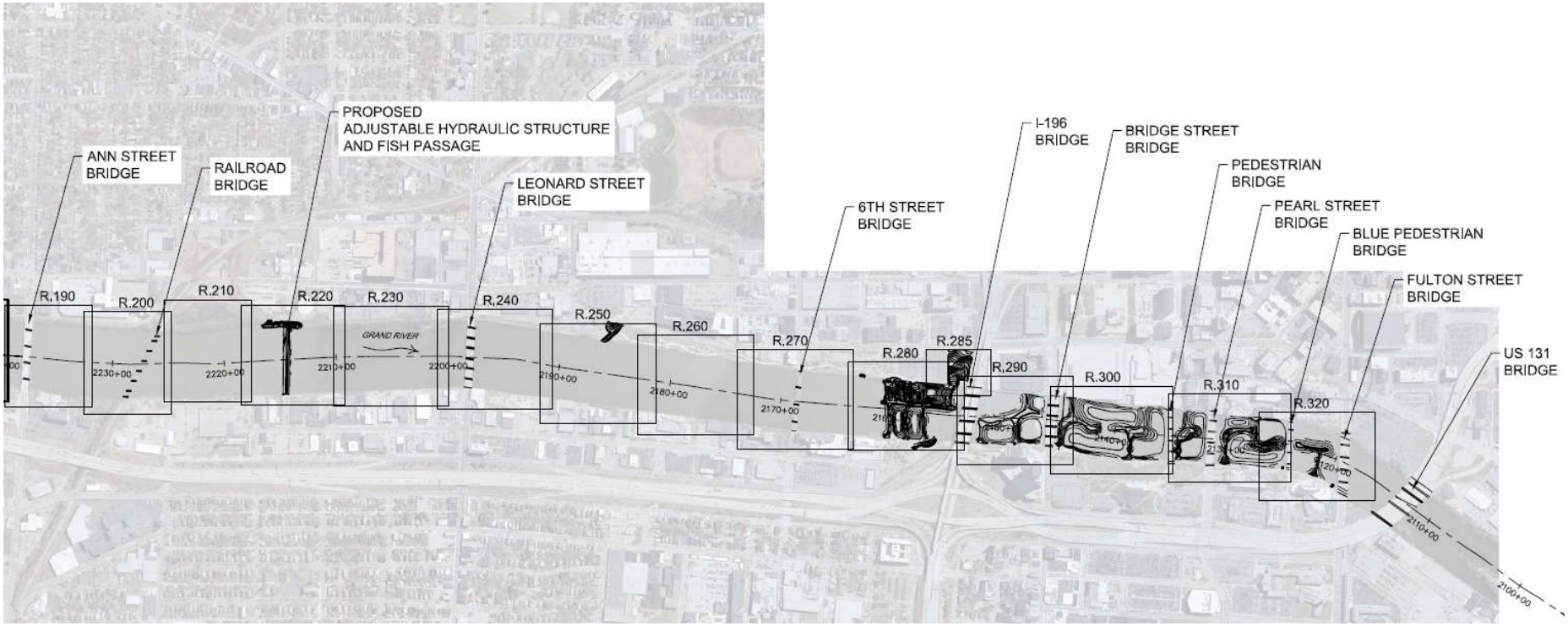

Figure 2. Proposed project conditions and location of AHS

2. SEA LAMPREY BLOCKAGE HYDRAULICS

The swimming capabilities of sea lamprey are jointly dependent on water temperature and velocity. Sea lampreys are anguilliform swimmers, oscillating both their tails and their heads simultaneously, and are considered relatively weak compared to other fish species (Beamish, 1974). Sea lampreys have a unique ability to adhere to surfaces through oral disc attachment which aids in their ability to migrate upstream by allowing periods of rest (McAuley, 1996).

Hydraulic conditions which exploit weak swimming traits to prevent passage have been investigated in multiple studies. Hunn and Youngs (1980) observed a series of structures which provided observed degrees of blockage and highlighted the hydraulic aspects which effectively restricted upstream passage of sea lamprey. They noted that the geometry of the structure crest and relative tailwater conditions were parameters which hindered migration. Observations for effective barriers included a free-overfall requirement of 1.5 ft at base flows, 0.5 ft at flood flows, and an overhanging crest lip requirement of 0.5 ft. Recommendations applied to the existing hydrology of the Grand River, elaborated upon by RiverRestoration (2016b), are presented in Figure 3. Free overfall is defined as the distance from the tailwater to crest elevation where aeration occurs at the crest of the structure.

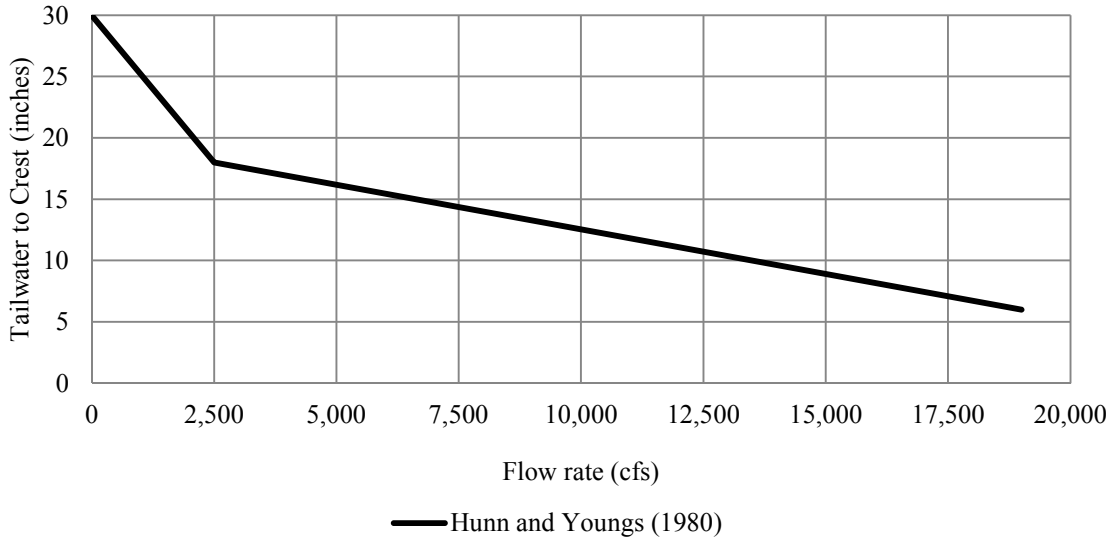

Figure 3. Hunn and Youngs (1980) vertical blockage observations applied to Grand River hydrology

McAuley (1996) performed flume studies on sea lamprey swimming burst and endurance velocities and compiled a number of other temperature-based studies for comparisons. Study results indicated a maximum burst speed for an adult sea lamprey at 13.1 ft/s (4 m/s) based on equations drawn from observations. McAuley (1996) developed two empirical equations of maximum distance (D_{max}) in a water velocity (V) and endurance time (t) for swimming speed (U). These observation data were for fish performance at temperatures between 14.3 and 21.0 °C. Endurance time for a specific swim velocity was noted to vary with temperature as illustrated in Figure 4 and Figure 5. In observations, water temperatures were required to exceed 16.5 °C for burst speeds to approach the maximum 13.1 ft/s. For water temperatures less than 10 °C, burst speeds did not exceed 5 ft/s (1.5 m/s). At burst speeds approaching 13.1 ft /s, maximum effort could only be sustained for less than two seconds. Endurance, or sustained, velocities were noted as 8.1 ft/s for approximately 10 ft of channel length.

Hanson (1980) investigated sea lamprey endurance and burst velocities in a flume study. The study indicated that burst velocities were on the order of 13 ft/s, yet may approach 15 ft/s in extreme cases. Sea lampreys were observed to not attempt any upstream passage at water temperatures less than 15.6°C. Results from Beamish (1974) reinforce findings from both McAuley (1996) and Hanson (1980); sea lamprey swimming speeds were found to be inversely related to water temperature. Beamish (1974) observed maximum sustained speeds at 1.16 ft/s (35.5 cm/s) at 15°C, the maximum temperature evaluated during the study.

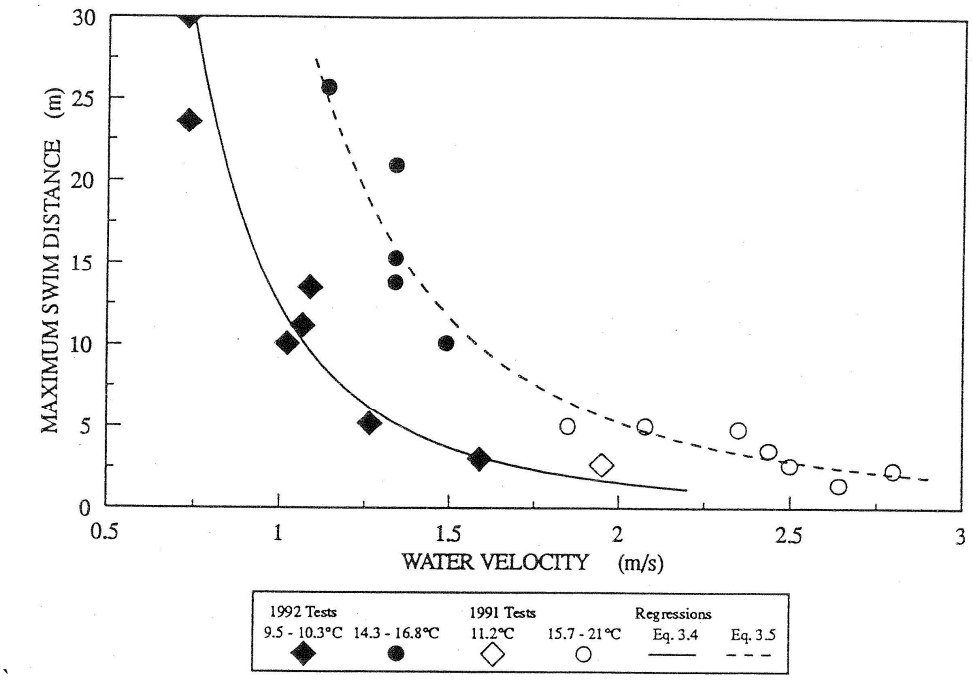

Figure 4. *Dmax* = 35.7 $V^{-2.77}$ McAuley (1996)

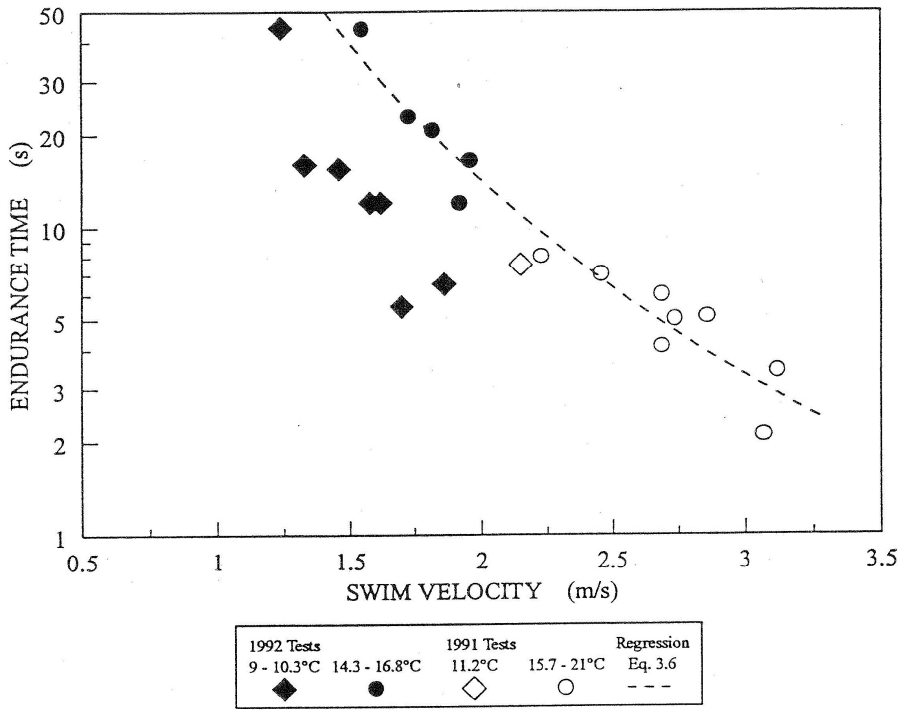

Figure 5. $T = 172.1\ U^{3.60}$ McAuley (1996)

Hydraulic design criteria were selected as vertical, free-overfall recommendations from Hunn and Youngs (1980) and velocity criteria from McAuley (1996). The AHS was optimized to produce either free-overfall conditions (greater than 1.5 ft, decaying to 1.0 ft at higher flows) or velocity conditions (13.1 ft/s burst or 8.1 ft/s over 10 ft sustained). The adjustability of the structure was incorporated to achieve blockage hydraulics while conforming to design constraints.

3. DESIGN CONSTRAINTS

Achieving hydraulic blockage criteria for the prevention of sea lamprey passage was constrained by a set of parameters within the river system. Free-overfall conditions assume that the crest of the structure be at least 0.5 ft from the tailwater in the channel and aerated, requiring passing fish to jump vertically out of the water to locate an upstream, quiescent hydraulic. When the tailwater in the main channel rises with increasing flow rates, the structure crest must gain elevation to maintain free-overfall criteria. At a certain flow rate and crest elevation of the structure, undesired upstream overbanking constraints will exist which restrict the operational range of the AHS. At this threshold, the AHS has the capacity to transition to a partial-crest configuration with lowered sections of the structure crest, meeting velocity blockage and overbanking design constraints. Additional constraining parameters not directly addressed in this report include run of the river, boat passage, and jumping fish passage.

The primary constraint on the operational range of the proposed AHS is the prevention of increasing the frequency of overbanking in the upstream reaches. Overbanking in the project reach occurs first at areas near North Park and Comstock Park where there exists trail infrastructure and residential properties at low-lying elevations which are inundated at elevations less than those resulting from the mean annual flood. The National Oceanic and Atmospheric Administration (NOAA) Advanced Hydrologic Prediction Service

indicated that a gage height at the USGS stream gage 04119000 of 14 ft corresponds to expected minor flooding within low-lying area at North Park and Comstock Park (NOAA, 2016). NOAA (2016) reported that the flow rate aligning with a gage reading of 14 ft is 16,400 ft^3/s. The expected minor overbanking elevation was estimated using a calibrated HEC-RAS Effective FEMA model from FTCH (2010) as 611.53 ft. Operation of the AHS was designed to fall below the overbanking elevation of 611.53 ft for all flow rates below 16,400 ft^3/s and to match the existing rating curve for flow rates exceeding 16,400 ft^3/s.

Run of the river is the nomenclature derived from a type of hydroelectric generation plant with little to no water storage. Michigan Department of Natural Resources (MDNR) defines run of the river as instantaneous inflow into the impoundment equaling instantaneous outflow. Facilities that do not adhere to run of the river stipulations will typically store and release volumes of water to generate hydroelectricity. Fluctuations in the downstream hydrology as a result of storage operations may result in considerable ecological impact (Anderson *et al.*, 2014). The project does not propose to impound, store, or pool water upstream of the AHS or have measurable effects on the downstream hydrograph. Due to the dynamic operational requirements to generate sea lamprey blockage hydraulics, the AHS will raise the upstream water surface to meet the free-overfall requirement or to build enough energy to meet velocity criteria. Recommended operations of the AHS were constrained to alter instream flow rates by no more than five percent. Five percent of the instream flow rate is within instrumentation error tolerances for discharge measurements within natural river channels (Rantz, 1982). Specifics of the unsteady flow control on the AHS will be accounted for during the mechatronic design of the structure.

Public interaction with the AHS is unavoidable and may take the form of boat passage, angling, or wading. Boat passage will be provided in a separate channel specifically designed to guideline shallow-draft watercraft. Boats may be line-guided through the passage channel from the shore through small hydraulic drops or have the option to portage around the AHS. During velocity configurations of the AHS, skilled navigation through the structure will be possible. Hydraulics through the passage channel were restricted to maximum velocities and minimum flow depths to safely float small boats. Specific hydraulics of the boat passage channel are detailed in RiverRestoration (2016c).

Passage of jumping fish species through the AHS is desired at all design flow rates. A fish ladder exists at the 6th Street Dam which allows for passage past the structure. Meeting or exceeding the performance of the existing fish ladder is a primary goal at the AHS. MDNR dictated specific criteria to be achieved for fish passage, including the height of the vertical jump, swim path to the jumping pool, depth of the jumping pool, peak velocities, attracting flows, and upstream flow control (MDNR, personal communication). A designated fish passage channel was designed as part of the AHS that meets MDNR criteria for all flow rates as detailed in RiverRestoration (2016c). Jumping fish may additionally utilize the boat passage channel and the overtopping crest of the AHS which increase in viability at higher flow rates.

4. AHS HYDRAULIC DESIGN

Design of the AHS to meet or achieve sea lamprey blockage hydraulics while remaining within design constraints utilized an iterative process which implemented various hydraulic models at different design stages. One-dimensional, two-dimensional, and three-dimensional numerical hydraulic models were applied based on necessary levels of hydraulic complexity. HEC-RAS models were used for one-dimensional, cross-sectionally averaged hydraulic determination in the downstream direction only (USACE, 2016). SRH-2D was used for depth-averaged, two-dimensional modeling in the downstream and lateral directions (Reclamation, 2008). FLOW-3D® was used for resolution of hydraulics in the downstream, lateral, and vertical directions (FlowScience, 2016). The design process of the AHS is described in the order of increasing hydraulic modeling complexity, detailing procedures and findings at each step.

4.1 One-dimensional hydraulic modeling

Proposed operations of the AHS meet either free-overfall or velocity blockage conditions for all design flow rates. During free-overfall conditions, the AHS will operate with the entirety of the structure crest in a uniform, complete configuration. Partial crest operation will lower sections of the AHS, directing flow to accelerate through the opening. HEC-RAS models were primarily employed to bracket the operational limits of both free-overfall and velocity configurations.

An Effective FEMA model was obtained from FTCH (2010) and modified to a Proposed Conditions model by including additional cross sections to represent the AHS and proposed channel modifications. The Proposed Conditions model included calibration of the downstream cross sections to surveyed water-surface data and bathymetry. Upstream of the 6th Street Dam, the Proposed Conditions model was calibrated to the Effective Model, with the inclusion of the proposed cross sections. Approximately 30 cross sections were added to the Effective Model to model the Proposed Conditions. The representation of the AHS in HEC-RAS incorporated 12 cross sections with blocked obstructions for structural piers and one inline structure comprised of eight gates. A gate coefficient of 3.6 was used as recommended by Obermeyer, Inc., the manufacturer of the steel gate structures utilized in the AHS design.

One-dimensional hydraulic modeling was used to iterate the baseline design of the AHS, including the footprint, sill shape and height where the gates would be seated, downstream ramp dimensions of the gates, and flow guiding structures. Modeling also determined upstream flood impacts and comparisons to existing conditions as detailed in RiverRestoration (2016a). Functionality of the AHS during partial-crest operations is dependent on fully-developed velocities across regions of the structure designed for velocity blockage hydraulics. Flow separation occurs at sharp interfaces which may allow regions within the AHS that sea lampreys may exploit for upstream passage. It was hypothesized that the inclusion of flow guiding structures would aid in smoothly transitioning flow to desired velocities without regions of reduced velocity and for more prolonged distance. Six, rounded guide-wall structures were included in the model as 5-ft blocked obstructions, creating seven individual flow paths with dimensions that could be later optimized. The bottom width of the main AHS structure, not including the boat passage channel and not including the 30-ft of blocked obstructions from the guide walls, was designed at 565 ft. Velocity magnitudes are a function of the head loss over a structure; the higher the difference between the upstream and downstream water-surface elevations, the greater the achieved velocity magnitude. The maximum height of the sill of the AHS with guide wall inclusions was found as 603.25 ft to not have an effect on the upstream 100-yr floodplain as determined from the Effective Model. The sill length and slopes downstream of the gates were optimized to generate the highest velocities during partial-crest operations.

The optimized sill geometry was evaluated one-dimensionally at the full range of potential conditions for complete-crest and partial-crest configurations to determine operational constraints. The complete HEC-RAS model used for analysis is provided in Electronic Appendix E.1. For the complete crest, the maximum operational discharge while adhering to Hunn and Youngs (1980) free-overfall barrier requirements was calculated at 10,000 ft^3/s while falling below the design constraint of a 611.53 ft water surface elevation at North Park Bridge for flow rates below 16,400 ft^3/s. Crest elevations were determined at incremental discharges leading up to 8,250 ft^3/s and 10,000 ft^3/s by adding 1.5 ft and 1.17 ft of vertical distance from the associated tailwater elevation, respectively. Simulations at identified crest elevations were performed for all discharges recommended for structure operation, ranging from 830 ft^3/s to 34,500 ft^3/s, and tabulated values were extracted for upstream water-surface elevations, change in energy head, Froude numbers, maximum velocities, distance of sustained 8.1 ft/s velocity, and crest to tailwater distance. Tabulated hydraulic values for complete crest operations are presented in Electronic Appendix E.2. Results indicated that complete-crest elevations may be operated to maintain free-overfall barrier hydraulics at all discharges below that used for the crest elevation determination; *e.g.* all flows less than 10,000 ft^3/s maintain free-overfall criteria at the

crest elevation optimized for 10,000 ft^3/s.

Transition to partial-crest operations requires incremental lowering of gate sections to accelerate flows through the guided channels. Optimization of the AHS for partial-crest operations focused on maximizing head differentials across the structure while maintaining overbanking design criteria. For a given flow rate, there exists an opening within the AHS where both head differential and velocities are maximized. To determine operational ranges, incremental values of gate openings ranging from 80-ft lowered to 360-ft lowered were evaluated across the full range of flow rates from 830 ft^3/s to 34,500 ft^3/s. For example, a lowered section of 360 ft corresponded to the required gate opening at 34,500 ft^3/s to fall within design constraints. For each combination of flow rate and gate opening, upstream water-surface elevations, change in energy head, Froude numbers, maximum velocities, distance of sustained 8.1 ft/s velocity, and crest to tailwater distance were tabulated as provided in Electronic Appendix E.2. Rough ranges of operation were determined from the modeling results and three gate configurations were found which functioned across a variety of flow rates. Configuration of the guided channels achieving openings of 260 ft, 340 ft, and 360 ft covered the partial-crest operational range from 10,000 ft^3/s to 34,500 ft^3/s.

4.2 Two-dimensional hydraulic modeling

One-dimensional modeling techniques are limited in the capability to capture variability in hydraulic parameters in the transverse direction. The AHS will produce significant deviations from one-dimensional hydraulics during partial-crest operation; transverse velocities gradients are expected to be on the order of 1 ft/s per linear foot or higher where conveyance is guided through designed pathways. Significant two-dimensional flow patterns affect the confidence in the one-dimensional model to produce accurate water-surface elevations immediately upstream of the AHS and to capture velocity magnitudes and distributions through gate openings. SRH-2D modeling of the AHS was performed to achieve the design of the guide-wall structures, spacing of the isolated channel bays, development of rating curves for the partial-crest openings of 260 ft, 340 ft, and 360 ft, determine the flow rates where the AHS will operate at various gate configurations, and ensure velocity criteria are achieved at operational thresholds.

Flow separation occurs at rapid channel transitions, such as the interface of a strong lateral flow component with a downstream component. Initial investigations of the AHS modeled the scenario of diverting all flows to the western region of the channel during partial-crest operations. Figure 6 and Figure 7 illustrate representative examples of velocity distributions under this management scenario. Interaction with the flow accelerating downstream through the opening and the lateral flow progressing alongside the raised gates promotes a condition where low-velocity separation zones occur at the lowered/raised gate interface. Velocities near the separation zones were modeled on the order of 8 ft/s maximum and not sustained for any significant distance, while peak and sustained velocity criteria in the main jet of flow surpassed sea lamprey blockage hydraulics. The separation zones are further problematic for sea lamprey passage due to the large back-eddy which forms at the downstream side of the raised gates. Flow separation creates regions of hydraulic weakness in the overall system which required investigation of structural additions and layout options to bolster uniformity.

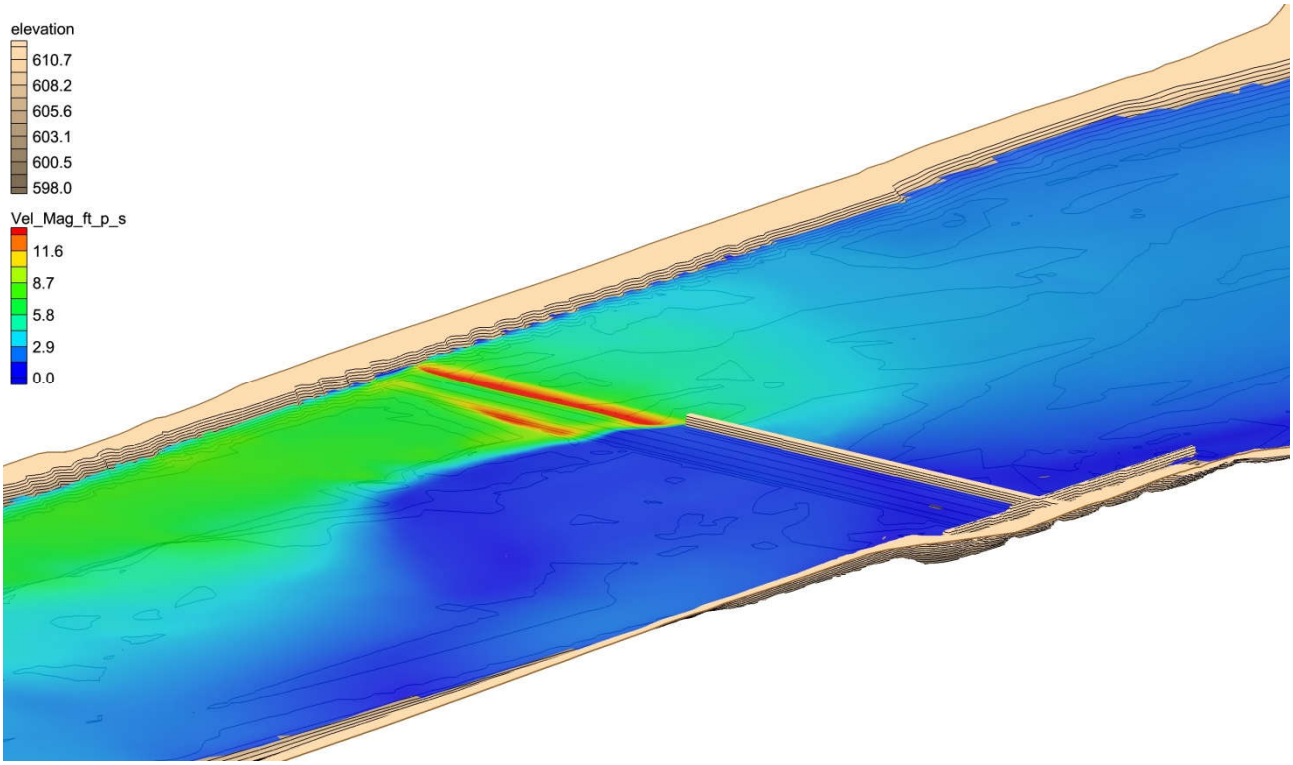

Figure 6. Velocity magnitude distribution, 10,000 ft^3/s with 260 ft down; flow down page; no guide-wall structures

Flow guide structures were investigated for inclusion to the AHS to smoothly transition flows and promote uniform, contained hydraulics along defined flow paths. Containing flows within guided channels forces sea lampreys to pass directly through focused hydraulics which is fundamental to meet successful velocity blockage. To divert flows smoothly into guided channels, various configurations of lowered gate sections were iteratively evaluated until a structural geometry was found to be effective at operational ranges indicated by the one-dimensional model (260 ft, 340 ft, 360 ft open). Guide-wall geometry drew inspiration from both airfoils and the Fibonacci sequence to transition flows as smoothly as possible. Raised gate sections in the middle of lowered gate sections serve to create backwater and incite flow separation upstream of the AHS. Table 1 details openings between the flow guide walls (AHS-1 through AHS-6, FL-1 through FL-3) with associated maximum gate heights. Figure 8 and Figure 9 illustrate the proposed layout of the AHS with guide-wall configurations. Gates designated fish ladder (FL) designed to operate for jumping fish species passage and boat passage gates are detailed in RiverRestoration (2016c).

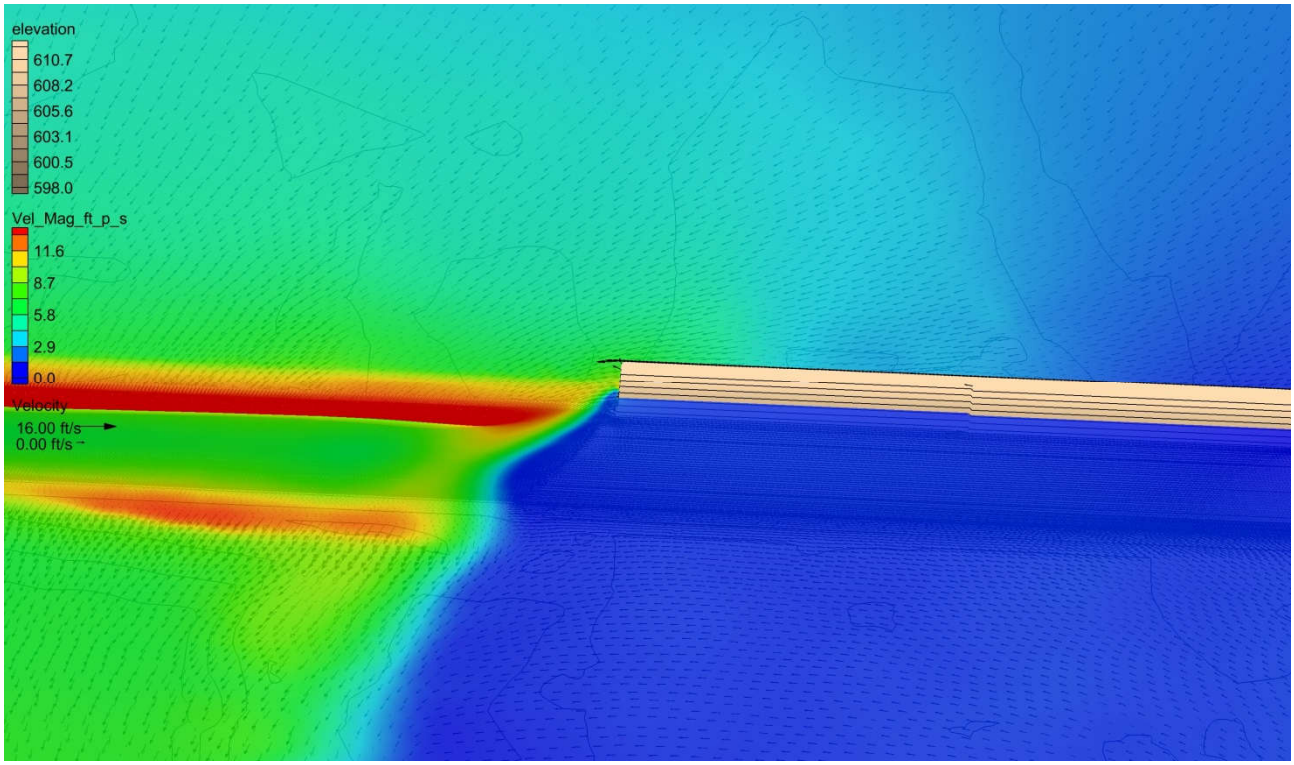

Figure 7. Velocity magnitudes and vectors, 10,000 ft^3/s with 260 ft down; flow down page; no guide-wall structures

Table 1. AHS opening and gate height dimensions

Opening	Width	Max gate elevation
-	ft	ft
AHS-1	80	611.7
AHS-2	55	611.7
AHS-3	130	607.7
AHS-4	80	611.7
AHS-5	130	607.7
AHS-6	70	611.7
FL-1, FL-2, FL3	20	611.7

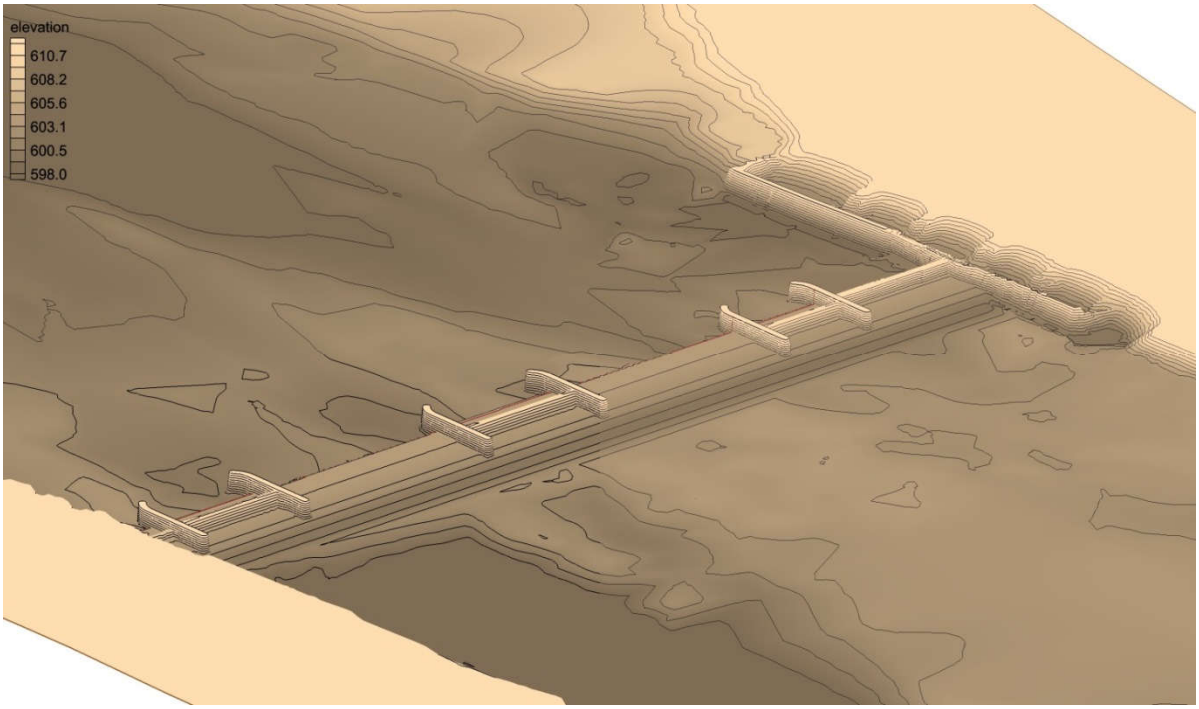

Figure 8. Finalized AHS design surface representation, perspective view

AHS-3 and AHS-5 conjunctively operate to create the required 260-ft opening in the structure while AHS-4 creates localized backwater initiating flow separation upstream of the structure. AHS-1 lowers after the 260-ft AHS-3 and AHS-5 configuration to create a 340-ft opening, with AHS-4 and AHS-2 serving as backwater influence. At the 360-ft down configuration, FL-1, FL-2, and FL-3 fully lower with AHS-6 functioning as backwater control. The guide walls were designed to transition flow into AHS-1, AHS-3, AHS-5, and FL-1 through FL-3 following the most efficient flow path possible. Deviation from recommended operation, such as operation of the even-numbered bays for velocity blockage, may result in flow separation at the guide walls and failure to meet design criteria.

A two-dimensional model of the AHS was created to evaluate depth-averaged velocities and water-surface elevations across the range of partial-crest operations. The model contained the AHS, an approach section of 1750 ft, and a downstream section of 2500 ft which includes the Leonard Street bridge piers. An irregular mesh was created to model hydraulics in SRH-2D with grid sizing ranging from 1 ft elements near the AHS to 10 ft elements in the approach section. Manning roughness values were set at 0.03 for the main channel and 0.02 for the AHS. A higher Manning value for the AHS crest and sill than typical for the steel and concrete materials it is comprised of was selected to account for vertical losses. Flow rates ranging from 10,000 ft^3/s to 34,500 ft^3/s were simulated until steady state conditions were achieved. Boundary conditions were specified from one-dimensional modeling results. Model mesh domains, input files, and output data are provided in Electronic Appendix E.3.

One-dimensional modeling provided rough discharge ranges for operation of the AHS. In order for thorough hydraulic modeling of the structure, the flow rates at which operations transition between bay configurations must be determined. At 10,000 ft^3/s, the complete crest transitions to 260-ft of dynamic gates by incrementally lowering AHS-3 and AHS-5 to maintain a water-surface elevation of 611.53 ft at North Park. To approximate the transition discharge, or the maximum flow permitted through the 260-ft down configuration, two-dimensional models of the AHS simulated water surface elevations upstream of the structure for flow rates of 10,000 ft^3/s to 16,400 ft^3/s to generate a stage discharge relationship as illustrated

in Figure 10. SRH-2D has been shown to predict upstream water-surface elevations for complex grade-control structures within approximately 5% of total flow depth (Gordon *et al.*, 2016). A separate stage-discharge relationship was generated through HEC-RAS to determine water-surface elevations upstream of the structure that correspond to the upstream overbanking requirements. Figure 11 illustrates the intersection of the two rating curves at 14,745 ft^3/s, which is the approximate flow which signals the transition from the 260-ft to the 340-ft configuration. Figure 12 and Figure 13 present rating curves for the 340-ft and 360-ft configurations. As illustrated in Figure 12, the stage-discharge relationship for the 340-ft configuration intersects overbanking design criteria at 16,400 ft^3/s, corresponding to the flow rate causing overbanking at existing conditions. The 340-ft configuration tracks existing condition water-surface elevations until approximately 19,000 ft^3/s, where the AHS transitions to the 360-ft configuration to maintain existing conditions.

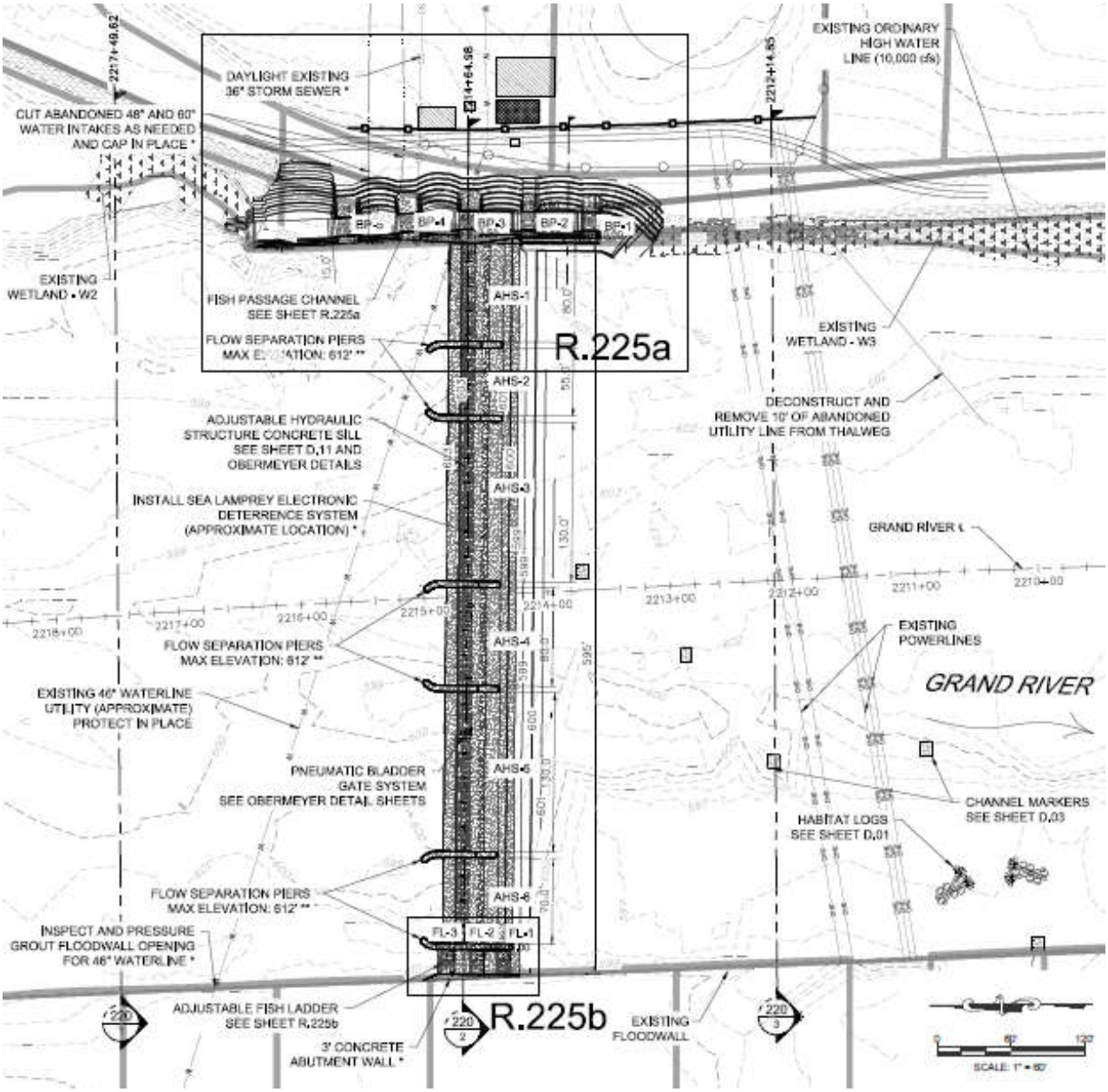

Figure 9. Finalized AHS schematic, plan view

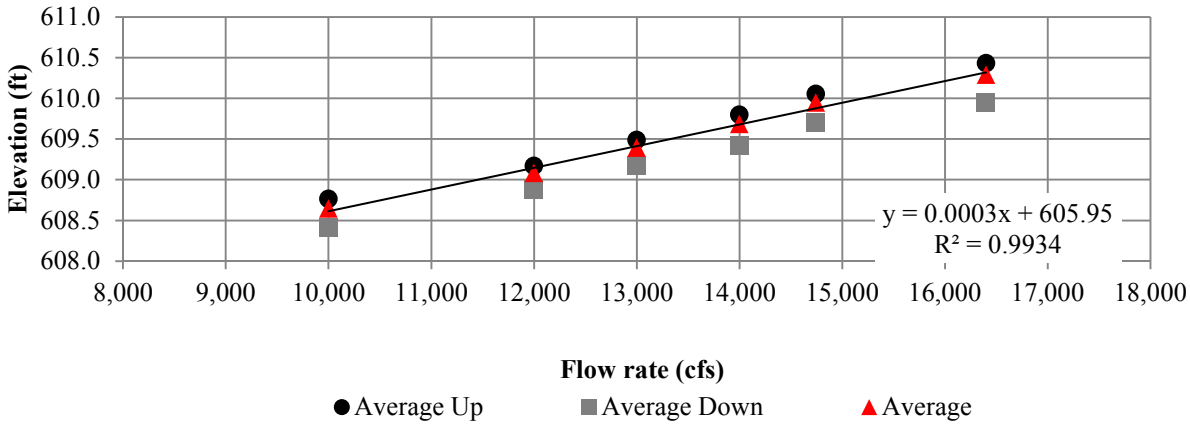

Figure 10. Stage-discharge relationship for AHS 260-ft down configuration

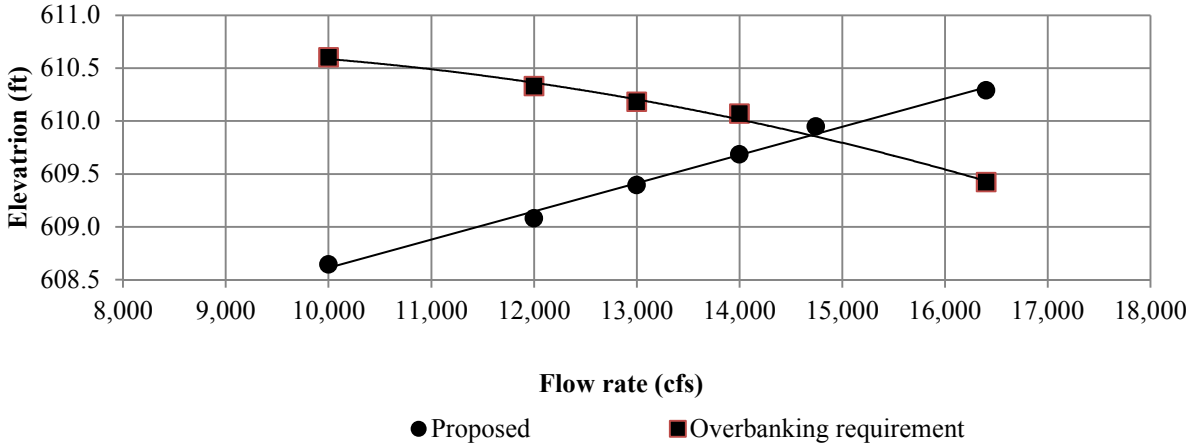

Figure 11. Intersection of rating curve and overbanking requirements for AHS 260-ft down configuration

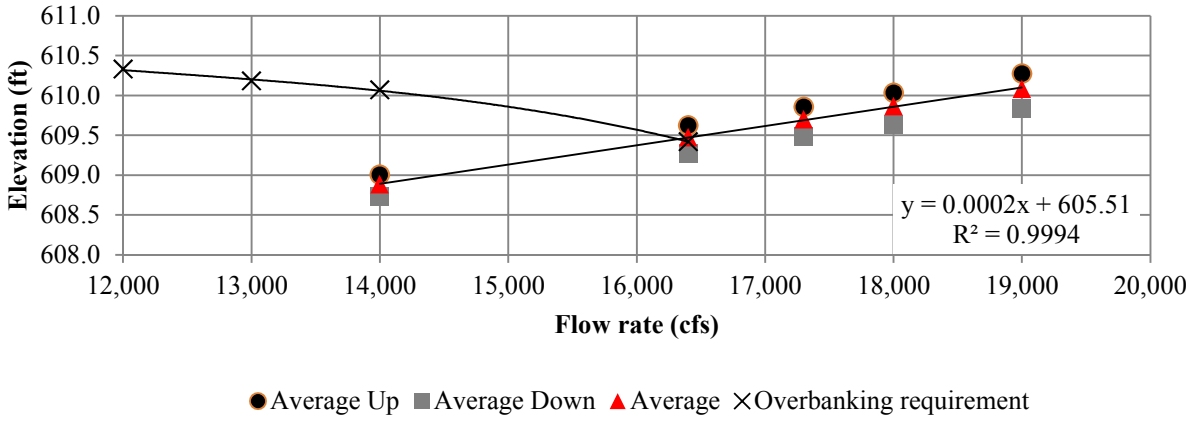

Figure 12. Stage-discharge relationship for AHS 340-ft down configuration

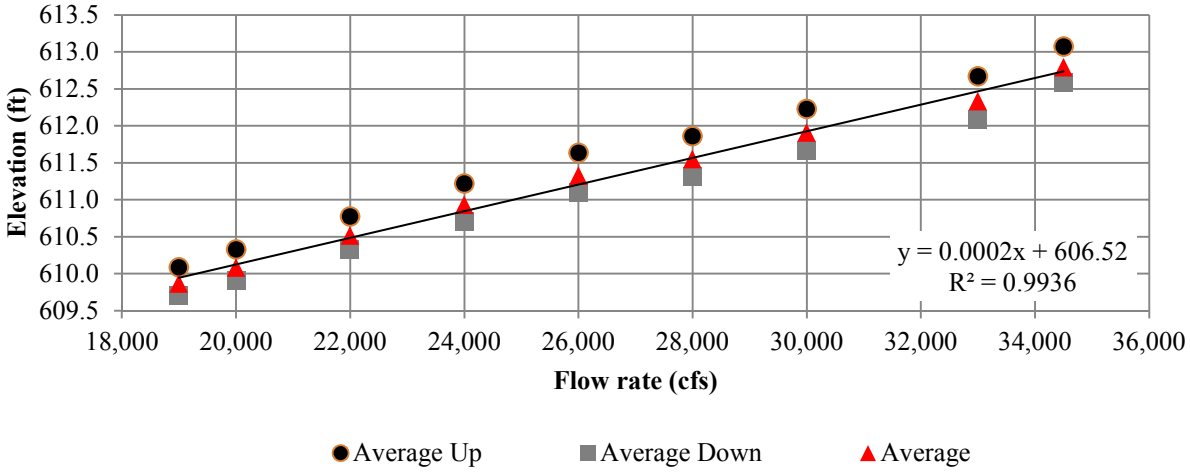

Figure 13. Stage-discharge relationship for AHS 360-ft down configuration

Rating-curve analysis identified transitional flows at 10,000 ft^3/s, 14,745 ft^3/s, and 19,000 ft^3/s. Ideal hydraulic conditions for velocity blockage dictate that the minimum and maximum flow rate for a given operational scenario meets design criteria. Modeling of the AHS at the subsequent configuration at each transitional flow was performed for conservative analysis of blockage hydraulics. Flow rates of 10,000 ft^3/s, 14,000 ft^3/s, 16,400 ft^3/s were evaluated at 260-ft down, 340-down, and 360-ft down, respectively. Figure 14 illustrates results of 10,000 ft^3/s passing through AHS-3 and AHS-5. Peak depth-averaged velocities were modeled as 16 ft/s, velocities exceeding 13.1 ft/s extended the full opening width, and approximately 40 ft of 8.1 ft/s was contained in the openings. Figure 15 illustrates results of 14,000 ft^3/s passing through AHS-1, AHS-3, and AHS-5. Peak depth-averaged velocities were modeled as 14.5 ft/s, velocities exceeding 13.1 ft/s extended the full opening width, and approximately 20 ft of 8.1 ft/s was contained in the openings. Figure 16 illustrates results of 19,000 ft^3/s passing through AHS-1, AHS-3, AHS-5, and FL-1 through FL-3. Peak depth-averaged velocities were modeled as 15 ft/s, velocities exceeding 13.1 ft/s extended fully across AHS-3 and AHS-5 and partially across AHS-1, and approximately 20 ft of 8.1 ft/s was contained in all structural openings.

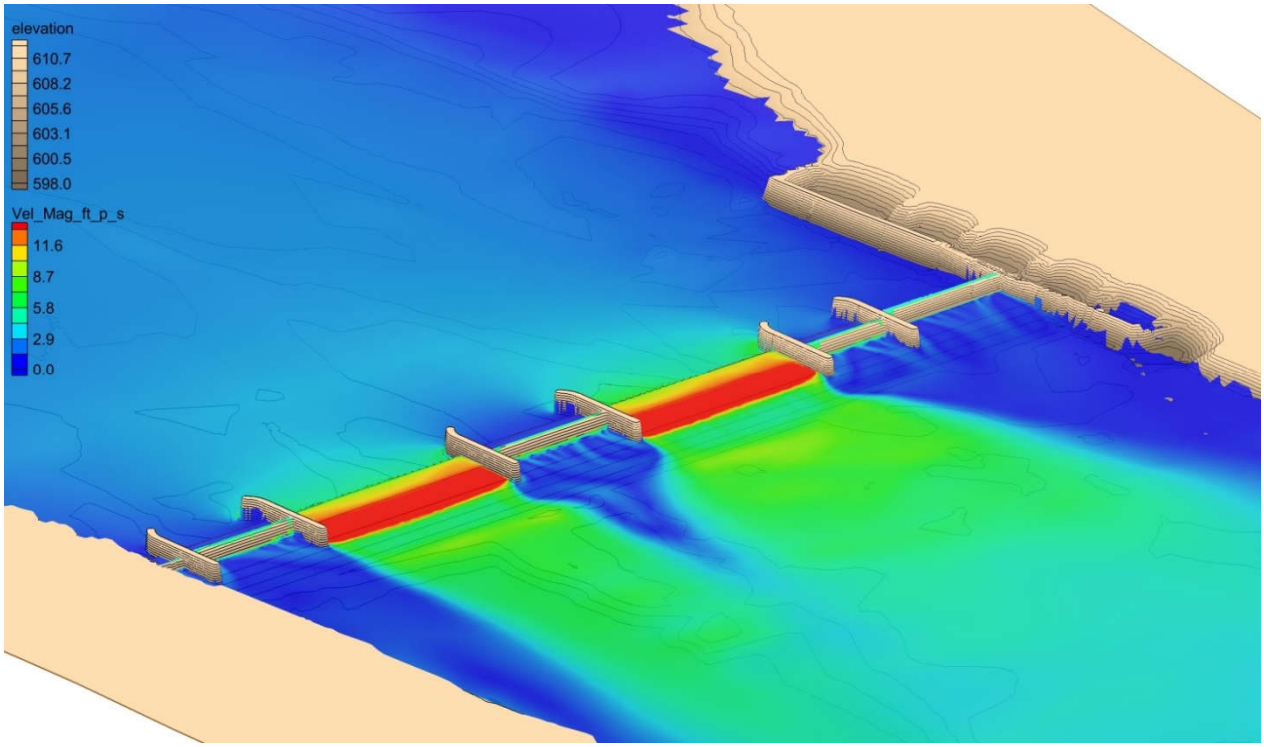

Figure 14. Velocity magnitude distribution, 10,000 ft^3/s at 260-ft down configuration, flow direction left to right

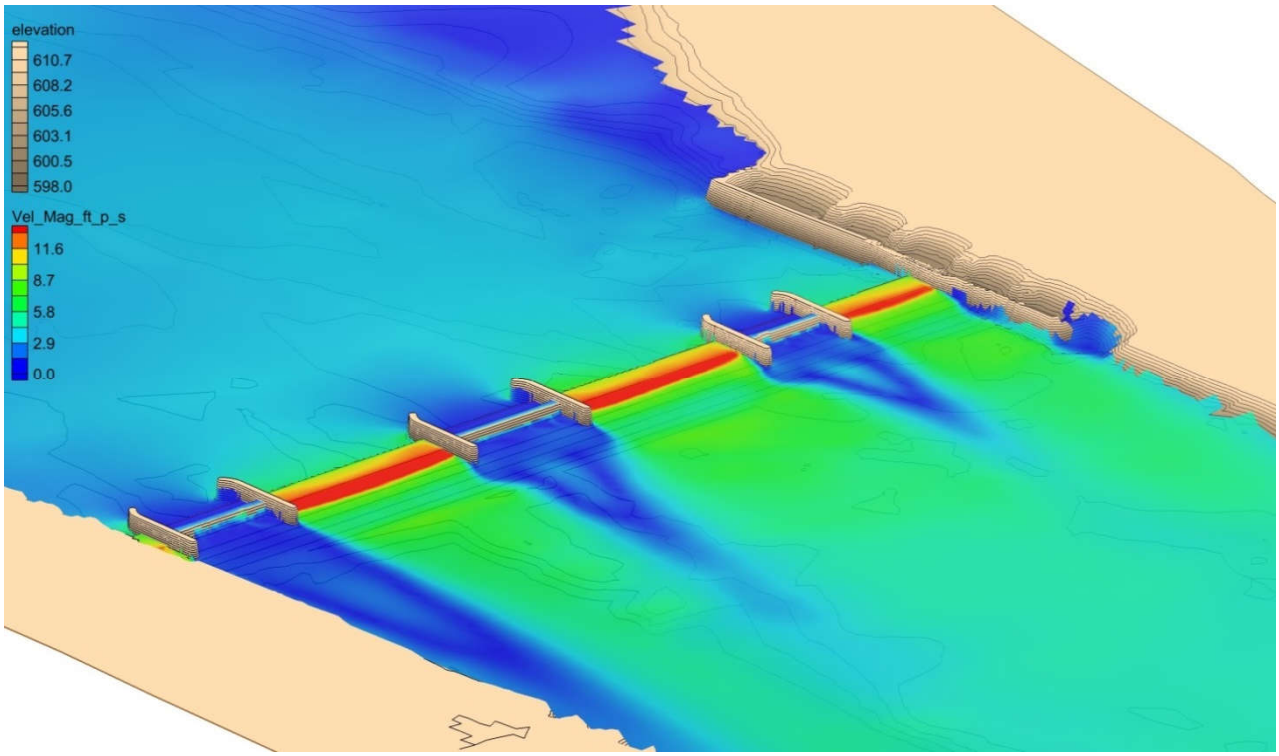

Figure 15. Velocity magnitude distribution, 14,000 ft^3/s at 340-ft down configuration, flow direction left to right

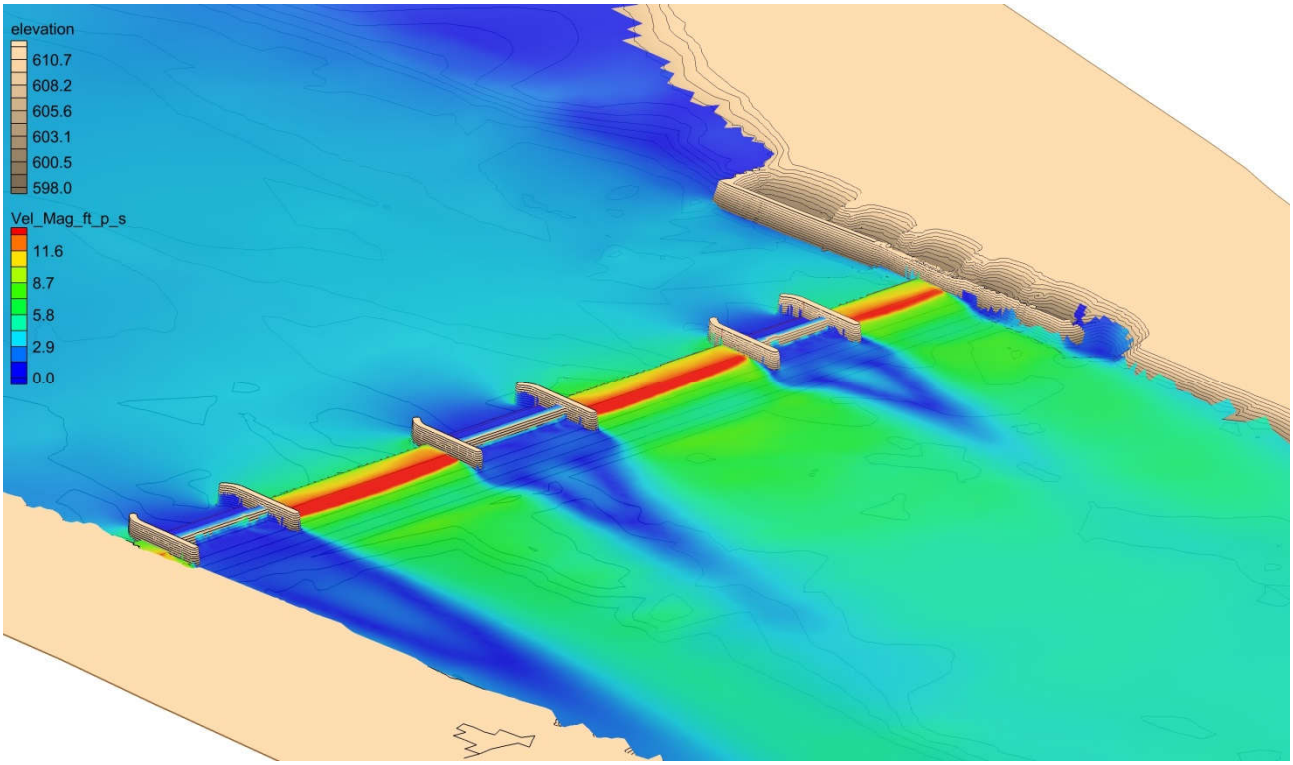

Figure 16. Velocity magnitude distribution, 19,000 ft^3/s at 360-ft down configuration, flow direction left to right

4.3 Three-dimensional hydraulic modeling

Two-dimensional modeling provided depth-averaged hydraulics, neglecting vertical flow components, which is appropriate for shallow water. When the vertical velocity component exceeds approximately 10% of the overall velocity magnitude, shallow-water assumptions are not valid and the vertical flow component must be addressed for an accurate solution. Significant vertical velocity components are expected during complete-crest configurations and during partial-crest operational transitions. Primary objectives of three-dimensional modeling were the determination of crest velocities for complete-crest operations, localized depressions in the tailwater from impinging jet flows, and transitional partial-crest operations.

A numerical simulation domain was established to evaluate three-dimensional structure hydraulics. A 10-ft wide section, 220 ft section of channel was modeled for backwatered flows to approach the transitional gate, overtop the crest, and interact with the tailwater. The numerical domain was split into a 120-ft approach section to the gate crest and a 100-ft section downstream to the tailwater. Grid sizing increased in resolution in the vicinity of the gate, and associated hydraulic gradients, ranging from 0.6 ft to 0.075 ft. Grid independence checks were performed by increasing the cell sizing by a factor of two and comparing overtopping jet velocities and backwatered elevations, the results of which are displayed in Figure 17. Percentage difference between the coarser mesh size and the simulation mesh size was less than 5%, ensuring that simulated hydraulics were independent of grid sizing.

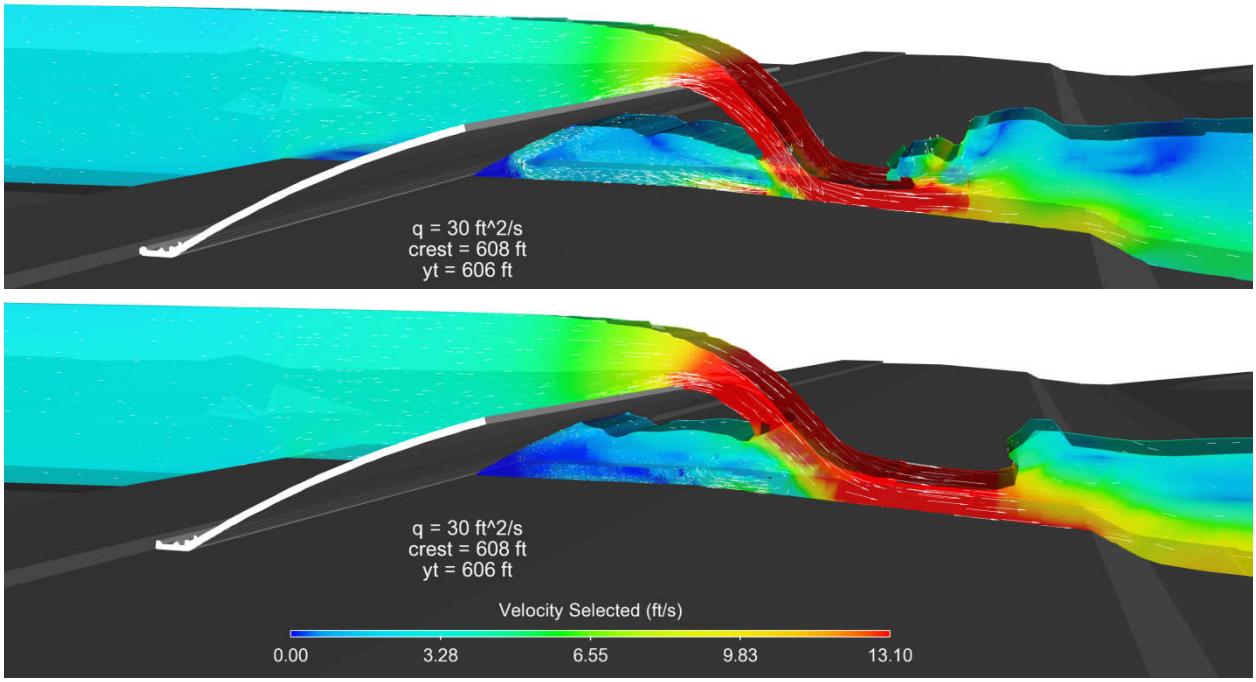

Figure 17. Simulation mesh (upper) and coarser independence mesh (lower) comparison

Specific hydraulics for recommended complete-crest operations are detailed in Figure 18. Aerated flow and effective free-overfall conditions were modeled under recommended operations. Flows passing over the crest of the gates accelerate to velocities exceeding burst-speed design criteria, impinge on the downstream concrete sill, and flow downstream at high velocities until interacting in a hydraulic jump with the tailwater. Flows travelling down the sill were designed to velocity magnitudes exceeding 13.1 ft/s. A sea lamprey attempting the barrier during complete-crest operations must pass a sustained distance of velocity exceeding burst-speed criteria before locating slower velocities underneath the jet. If successful in traveling to the slower zone underneath the gate, upstream passage would necessitate jumping a height greater than free-overfall criteria into a jet of water which exceeds burst speeds. Model results emphasize the effective nature of the complete-crest operation, as both a free-overfall and velocity barrier.

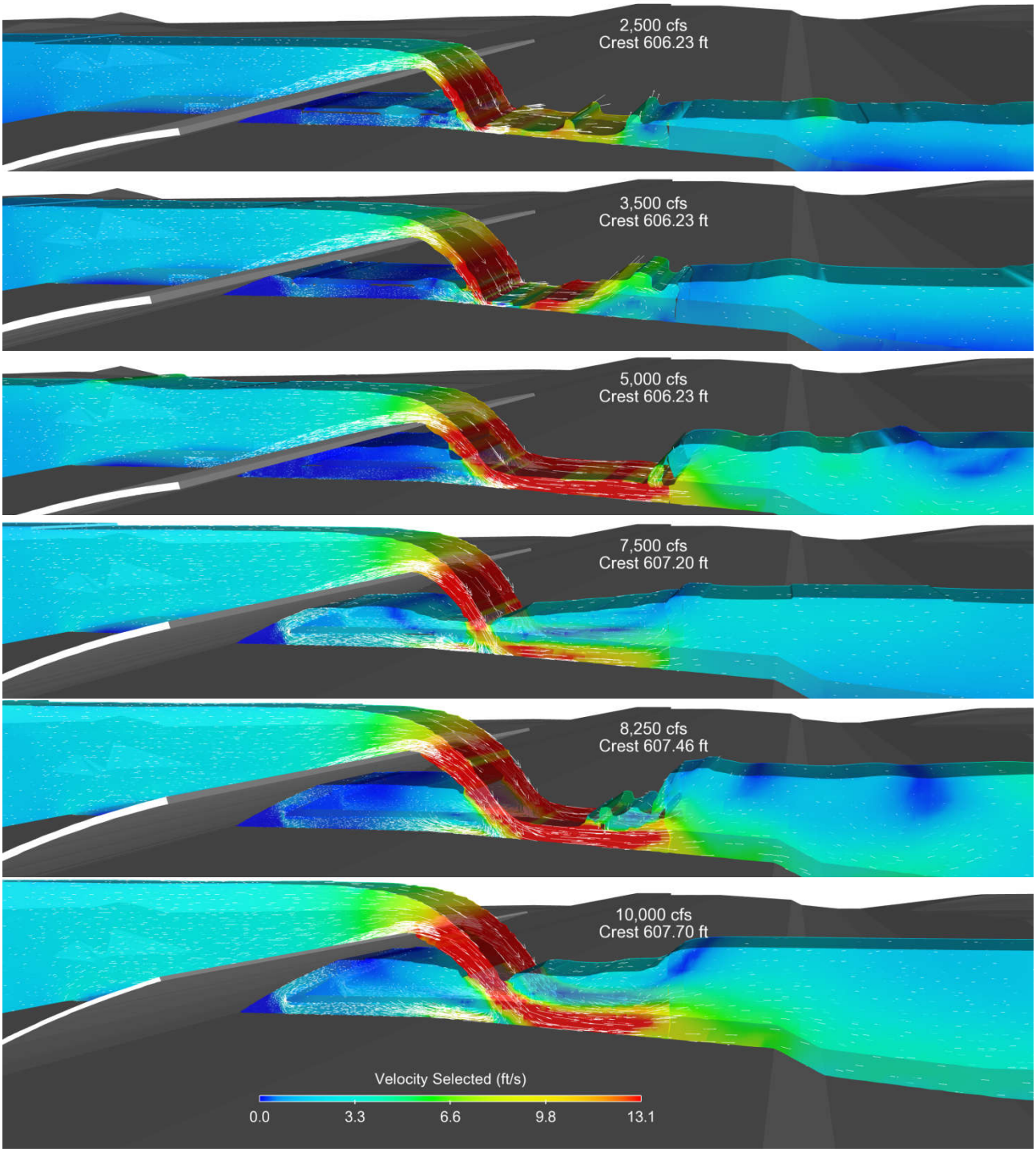

Figure 18. Complete crest operations; flow direction left to right

Lowering of the transitional gates to achieve the 260-ft, 340-ft, and 360-ft configurations will transition the operational function of the structure from free-overfall to velocity blockage. Gates lower incrementally with

increasing discharge to maintain the upstream overbanking design constraint and run-of-river requirements. Flow over the gate crest increases to a maximum value when the gates are fully lowered; however, tailwater influences the magnitude and shape of the impinging velocity jet. Overtopping flows were examined to ensure blockage design was achieved through the transitional operations.

Maximum flow rates through the lowered sections were ascertained from the two-dimensional model as approximately 50 ft^3/s per linear foot of sill for the 260-ft and 340-ft configurations, and up to 70 ft^3/s per linear foot for the 360-ft configuration. Tailwater elevations for the transitional partial-crest operations were taken from one-dimensional results ranging from 606.52 ft (10,000 ft^3/s) to 608.96 ft (20,000 ft^3/s), or the full range of transitional tailwater elevations. Elevations of the gate crests have a range from 611.70 ft at the fully raised position, to 603.25 at the fully lowered position. Due to the curved design of the gate, an elevation of 604.52 ft corresponds to a gate crest parallel to the sill. A test matrix was design based on the transitional operation parameter ranges of the system. Four crest elevations (610 ft, 608 ft, 606 ft, and 604.52 ft), four unit discharges (20 ft^2/s, 30 ft^2/s, 40 ft^2/s, and 50 ft^2/s), and three tailwater elevations (610 ft, 608 ft, and 606 ft) were combined into 48 individual test configurations for numerical evaluation. Configurations were given the nomenclature G for gates, Q for total modeled discharge, and T for tailwater; e.g. configuration 610G_200Q_610T would correspond to a gate elevation of 610 ft, a discharge of 200 ft^3/s, and a tailwater elevation of 610 ft.

Simulations were evaluated until steady state conditions were achieved for all configurations. Pertinent data for sea lamprey blockage were extracted from simulation results, including free-overfall height, distance from the trough of the jet to the crest elevation, average jet velocity, maximum jet velocity, and total jet distance. Important hydraulic parameters to AHS operations include backwatered upstream water surface elevations and piezometric head loss through the structure. A schematic of flows overtopping the transitional gates with identified parameters is presented in Figure 19. Table 2 presents the test configurations and summary of data extracted from the numerical model. Results indicated that hydraulics achieved either free-overfall or velocity barrier criteria for the majority of configurations evaluated. Configurations which did not meet blockage design criteria extended beyond designed hydraulic conditions; tailwater elevations were typically 610 ft, which exceeds the maximum tailwater elevation at 20,000 ft^3/s of 608.96 ft.

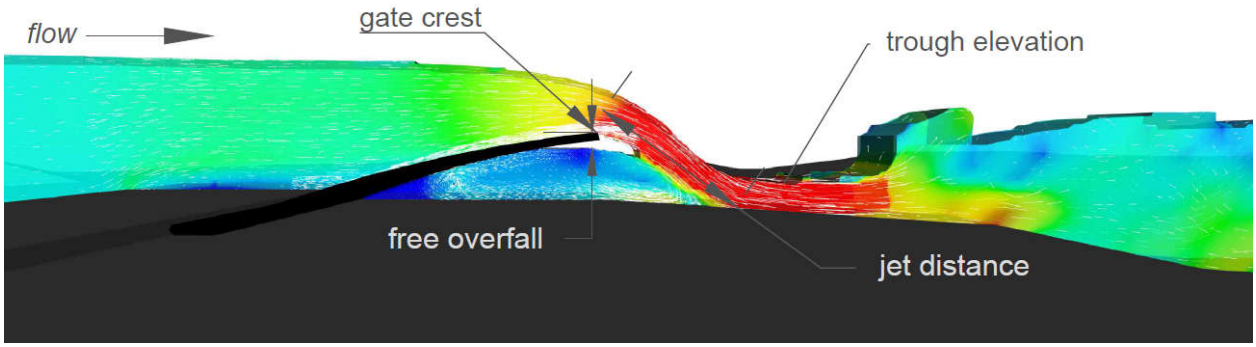

Figure 19. Partial-crest overtopping flow schematic with parameters identified

Table 2. Transitional gate configurations and results

Configuration	Meets criteria	Free-overfall height	Trough to crest	Avg. jet velocity	Max jet velocity	Jet distance	US WSE	Piezo. head loss
-	-	*ft*	*ft*	*ft/s*	*ft/s*	*ft*	*ft*	*ft*
610G_200Q_610T	*Yes*	2.5	1.7	16.4	17.8	12.7	612.7	2.7
610G_300Q_610T	*Yes*	2.8	3.2	17.7	20.1	13.7	613.7	3.7
610G_400Q_610T	*Yes*	2.7	3.0	18.7	21.9	15.8	614.4	4.4
610G_500Q_610T	*Yes*	2.9	4.9	20.1	22.4	16.4	615.2	5.2
610G_200Q_608T	*Yes*	3.1	3.0	15.4	17.6	10.9	612.7	4.7
610G_300Q_608T	*Yes*	3.1	3.9	17.4	19.2	13.0	613.7	5.7
610G_400Q_608T	*Yes*	3.1	4.2	18.4	21.1	14.9	614.4	6.4
610G_500Q_608T	*Yes*	2.8	4.2	19.5	22.1	15.9	615.2	7.2
610G_200Q_606T	*Yes*	4.9	4.4	17.1	19.0	10.5	612.7	6.7
610G_300Q_606T	*Yes*	4.6	5.4	17.2	20.9	11.9	613.6	7.6
610G_400Q_606T	*Yes*	4.6	5.5	19.3	22.8	12.9	614.4	8.4
610G_500Q_606T	*Yes*	4.0	6.6	20.6	23.9	14.3	615.2	9.2
608G_400Q_610T	*Yes*	0.0	-0.5	14.9	16.9	16.0	612.6	2.6
608G_500Q_610T	*Yes*	0.0	-0.5	17.8	18.4	15.6	613.3	3.3
608G_200Q_608T	*Yes*	1.7	1.7	14.5	15.7	9.4	610.8	2.8
608G_300Q_608T	*Yes*	1.7	2.0	16.1	17.3	11.0	611.8	3.8
608G_400Q_608T	*Yes*	1.6	3.0	17.1	18.5	12.9	612.6	4.6
608G_500Q_608T	*Yes*	1.7	2.9	19.1	20.8	13.0	613.3	5.3
608G_200Q_606T	*Yes*	2.9	1.1	15.4	16.5	8.3	610.8	4.8
608G_300Q_606T	*Yes*	3.8	4.5	17.4	20.2	10.1	611.7	5.7
608G_400Q_606T	*Yes*	3.1	4.1	18.7	21.1	10.5	612.5	6.5
608G_500Q_606T	*Yes*	2.4	4.3	19.9	21.4	13.1	613.4	7.4
606G_500Q_610T	*Yes*	0.0	-1.9	14.9	15.2	17.8	611.7	1.6
606G_300Q_608T	*Yes*	0.0	-0.5	13.0	13.8	12.3	610.0	2.0
606G_400Q_608T	*Yes*	0.0	-1.8	15.0	15.6	12.9	610.8	2.8
606G_500Q_608T	*Yes*	0.0	-1.1	17.3	18.1	17.3	611.5	3.5
606G_200Q_606T	*Yes*	1.2	0.2	14.3	15.2	7.0	608.9	2.9
606G_300Q_606T	*Yes*	1.6	2.5	15.8	16.9	8.3	609.9	3.9
606G_400Q_606T	*Yes*	0.2	2.0	18.0	19.7	9.3	610.7	4.7
606G_500Q_606T	*Yes*	0.0	1.1	18.6	20.7	11.0	611.5	5.5
604.52G_500Q_610T	*Yes*	0.0	-4.7	13.7	14.7	16.4	610.8	0.8
604.52G_300Q_608T	*Yes*	0.0	-2.3	12.6	13.6	9.1	609.4	1.4
604.52G_400Q_608T	*Yes*	0.0	-1.7	14.5	15.3	12.9	609.7	1.7
604.52G_500Q_608T	*Yes*	0.0	-3.0	14.7	16.3	17.4	610.5	2.5
604.52G_200Q_606T	*Yes*	0.0	0.3	13.7	14.6	9.7	608.0	2.0
604.52G_300Q_606T	*Yes*	0.0	-0.8	14.0	14.8	14.0	608.9	2.9
604.52G_400Q_606T	*Yes*	0.0	-0.8	15.4	16.5	15.2	609.9	3.9
604.52G_500Q_606T	*Yes*	0.0	-1.4	15.7	16.6	18.5	610.2	4.2
608G_200Q_610T	*No*	n/a	n/a	n/a	n/a	n/a	n/a	n/a
608G_300Q_610T	*No*	n/a	n/a	n/a	n/a	n/a	n/a	n/a
606G_200Q_610T	*No*	n/a	n/a	n/a	n/a	n/a	n/a	n/a
606G_300Q_610T	*No*	n/a	n/a	n/a	n/a	n/a	n/a	n/a
606G_400Q_610T	*No*	n/a	n/a	n/a	n/a	n/a	n/a	n/a
606G_200Q_608T	*No*	n/a	n/a	n/a	n/a	n/a	n/a	n/a
604.52G_200Q_610T	*No*	n/a	n/a	n/a	n/a	n/a	n/a	n/a
604.52G_300Q_610T	*No*	n/a	n/a	n/a	n/a	n/a	n/a	n/a

Configuration	Meets criteria	Free-overfall height	Trough to crest	Avg. jet velocity	Max jet velocity	Jet distance	US WSE	Piezo. head loss
-	-	*ft*	*ft*	*ft/s*	*ft/s*	*ft*	*ft*	*ft*
604.52G_400Q_610T	*No*	n/a	n/a	n/a	n/a	n/a	n/a	n/a
604.52G_200Q_608T	*No*	n/a	n/a	n/a	n/a	n/a	n/a	n/a

Specific determination of crest elevations of the transitioning gates and overflowing discharges during partial-crest operations required the development of a stage-discharge rating curve from the results in Table 2. Obermeyer (2016) recommends that the stage-discharge relationship for gates similar to the AHS follow the format of Equation 1 with coefficient *C* following the format of Equation 2.

$$\boldsymbol{Q = Cw(H \quad h)^{1.5}} \tag{1}$$

$$\boldsymbol{C = C_o + \left(\frac{h - h_{min}}{h_{max} - h_{min}}\right)(C_c \quad C_o)} \tag{2}$$

where:
Q = volumetric flow rate;
C = discharge coefficient;
w = spillway gate width;
H = upstream flow depth;
h = distance from gate crest to bed;
C_o = discharge coefficient in lowered position;
C_c = discharge coefficient in raised position;
h_{min} = top-of gate elevation in lowered position; and
h_{max} = top of gate elevation in raised position.

Obermeyer (2016) recommends that values of C_c and C_o be set at 3.6 $ft^{0.5}/s$ and 3.3 $ft^{0.5}/s$, respectively, based on undisclosed scaled physical model testing. No information pertaining to the gate layout, shape, or orientation was provided for context of the applicability of Equation 1 and Equation 2 to the AHS. Data acquired during the numerical modeling test matrix was sufficient to develop tailored versions of Equation 1 and Equation 2 to the operation of the AHS. The value of C was found for each gate elevation by finding the linear-regression slope of Q plotted with $(H - h)^{1.5}$ as illustrated in Figure 20. Coefficients of determination were on the order of 0.90 or higher for the linear regressions. Values of C for the 610 ft gate, 608 ft gate, 606 ft gate, and 604.52 ft gate were 4.26, 3.99, 3.38, and 3.30, respectively. Using minimum and maximum C and h values for the AHS from the numerical model with Equation 1 and Equation 2, flow rates passing over the AHS gates was predicted with a coefficient of determination of 0.94 and mean-average-percent-error of 6.37%. Using values from Obermeyer (2016), flow rates were estimated at a coefficient of determination of 0.74 and mean-average-percent-error of 14%

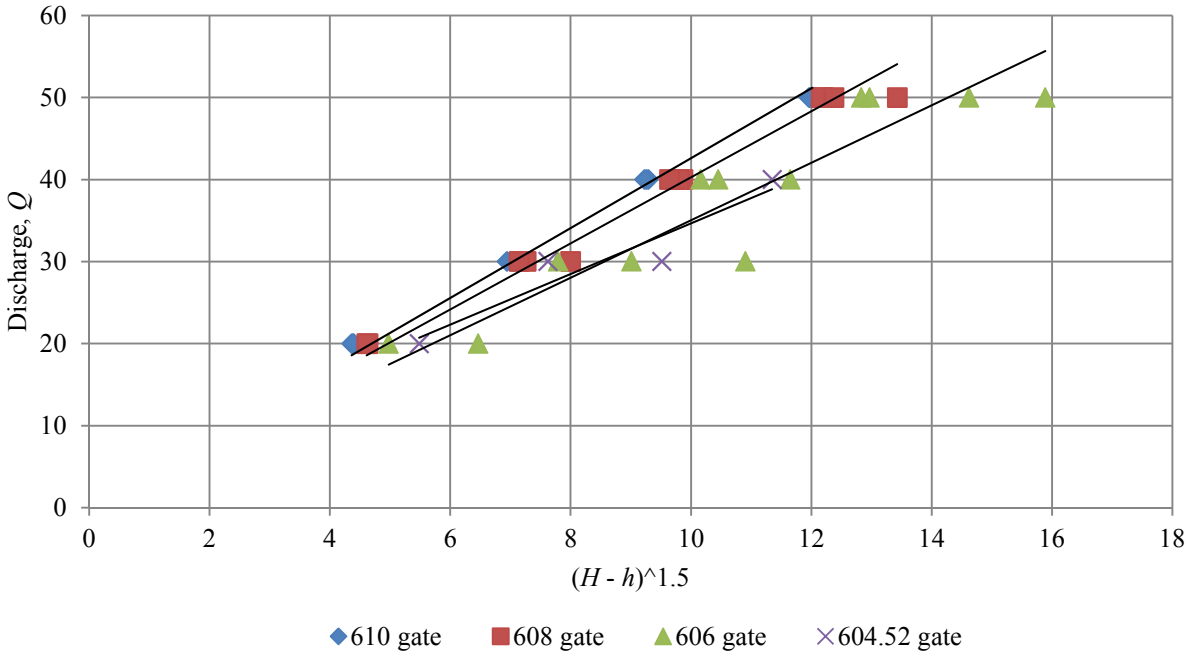

Figure 20. Stage-discharge relationships for evaluated gate elevations

Maximum and average jet velocities were examined as a function of independent parameters from the transitional gate matrix. Factors potentially impacting jet velocities include the flow rate, crest orientation angle and elevation, presence of aeration, or tailwater elevation. Examination of independent parameters indicated that the piezometric head difference, or the elevation difference between the upstream and downstream water surfaces, was the only variable which significantly affected velocity magnitudes. Figure 21 illustrates the linear relationship of average jet velocity with head difference and 95% confidence intervals and Figure 22 illustrates similar results for the maximum jet velocity. Relationships of velocity and head loss provide useful tools to approximate hydraulics through the range of transitional AHS operations. Velocity functions were developed with effective configurations as indicated in Table 2. Gate crests below 608 ft with tailwater elevations exceeding 610 ft were found to not achieve velocity blockage criteria and were discarded from predictive relationship calculations.

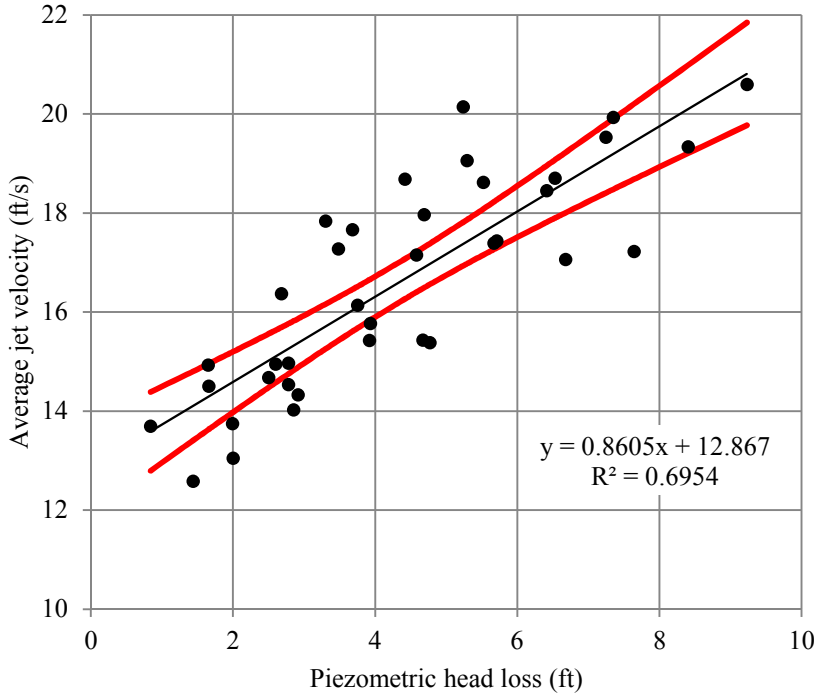

Figure 21. Average jet velocity near crest as a function of head loss with 95% confidence intervals

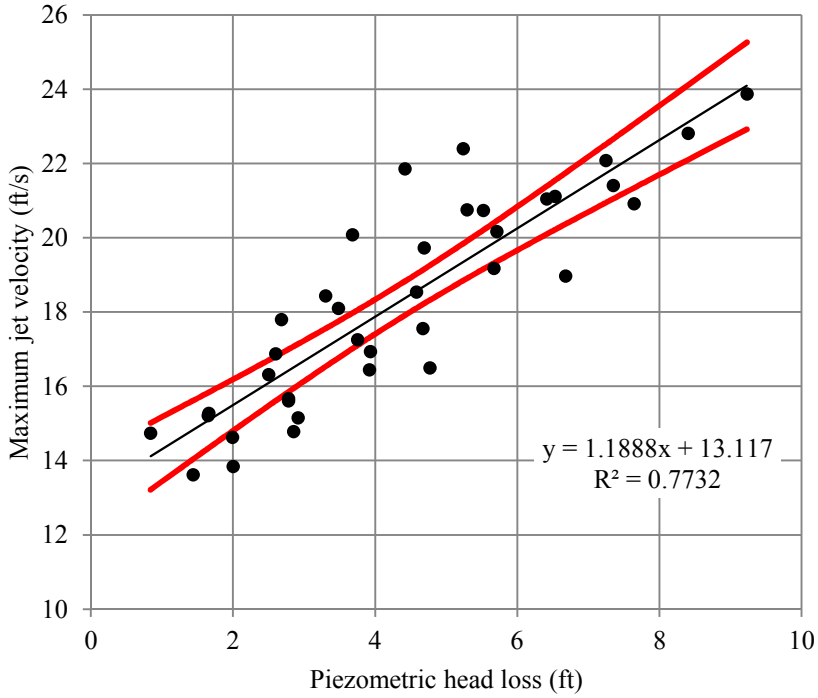

Figure 22. Maximum jet velocity near crest as a function of head loss with 95% confidence intervals

Given known ranges of unit discharge for each transitional bay, with associated start and end of transition

headwater and tailwater constraints, the stage-discharge and velocity relationships developed from the three-dimensional model results were applied to determine the crest elevations and velocities during transitional operations. Figure 23, Figure 24, and Figure 25 illustrate headwater, tailwater, applicable calculated average and maximum velocities, and calculated crest elevations for the transitional operations. Velocities for the 360-ft transition were not calculated as tailwater values fell outside of the range of the predictive relationship. As the crests lower, it is illustrated that velocities decrease due to the lowering of piezometric head difference; however, depth-averaged velocities within the overtopping jet are expected to exceed 13.1 ft/s at the crest for all flow conditions during gate transitions.

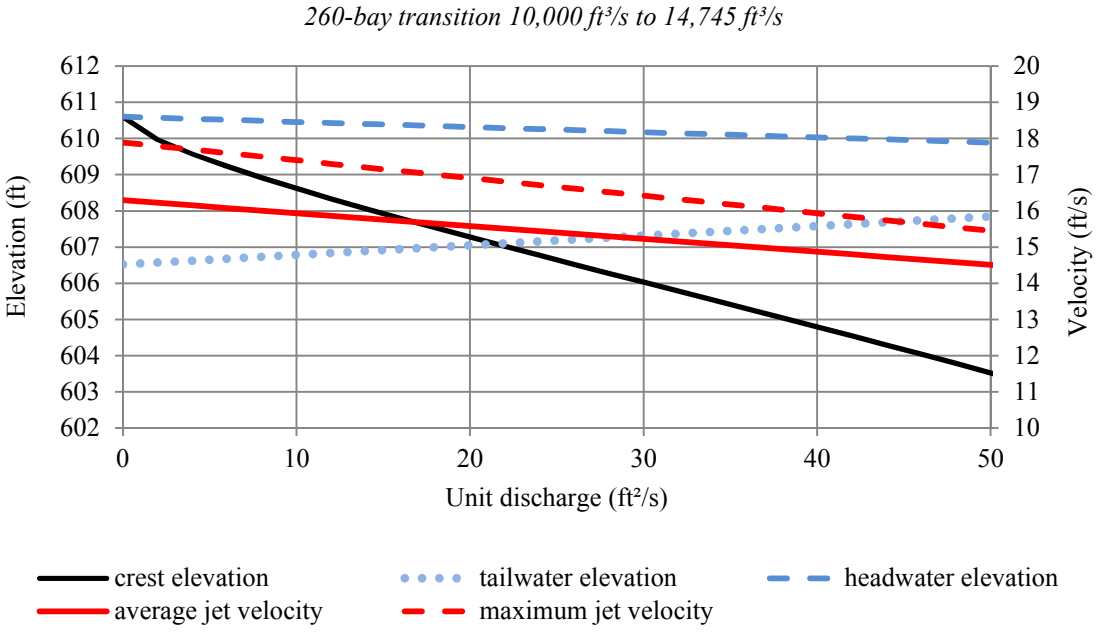

Figure 23. 260-ft configuration transitional hydraulics

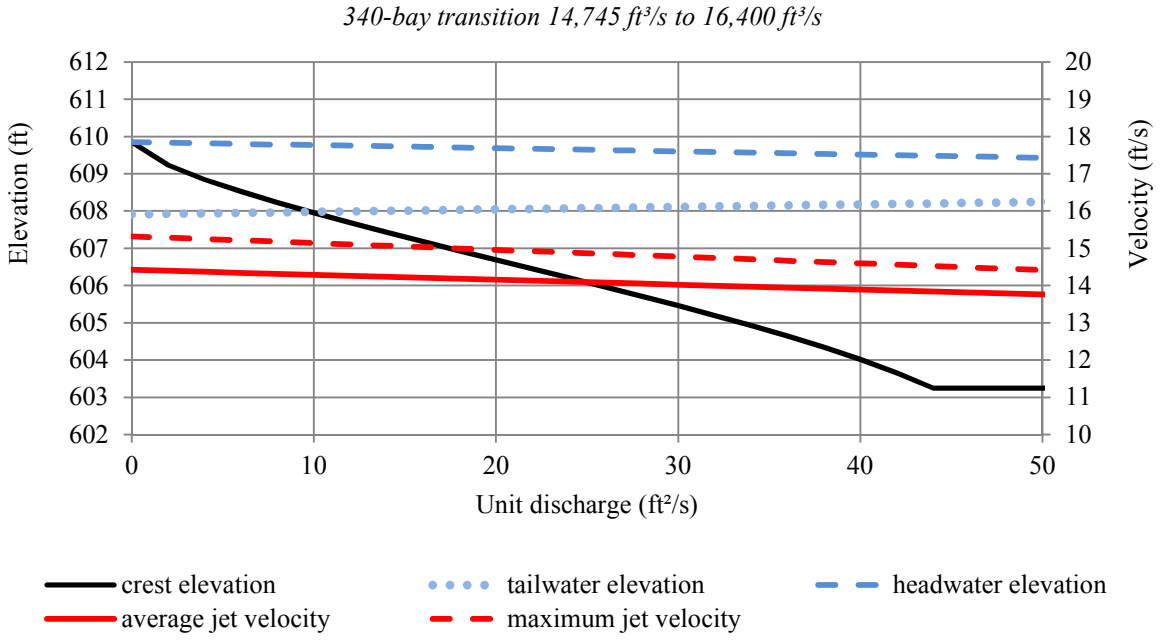

Figure 24. 340-ft configuration transitional hydraulics

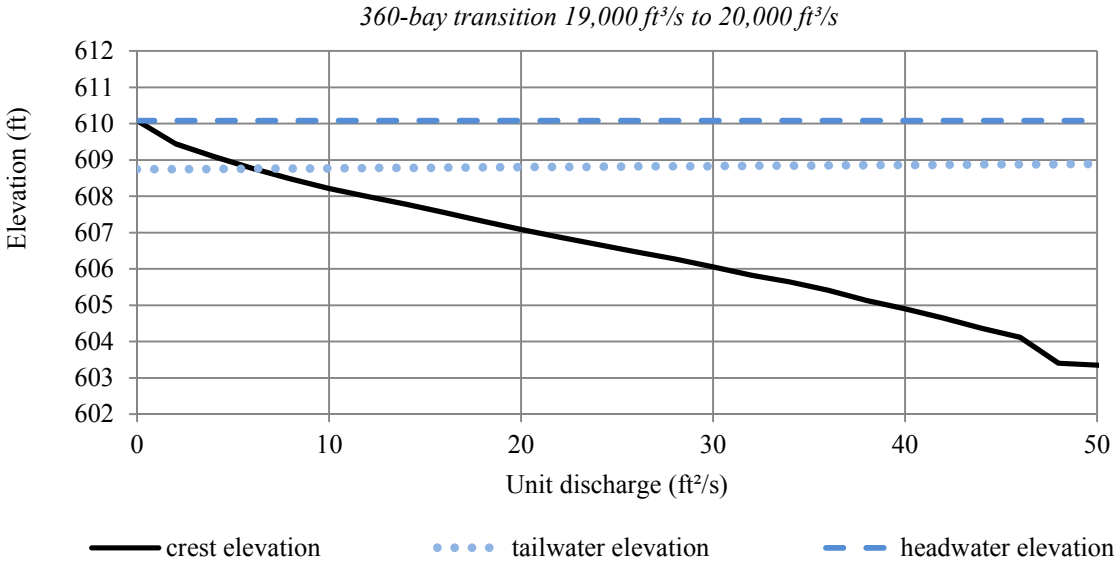

Figure 25. 360-ft configuration transitional hydraulics

Verification simulations were examined for the three transitional operations to validate results and barrier functionality. Minimal velocity configurations were the focus of verifications, identified by the crest falling below the tailwater elevation with relatively low unit discharge passing over the crest. At the 260-ft transition, configuration 606G_300Q_608T and 604.52G_400Q_608T correspond well to the expected

operational conditions displayed in Figure 23. Velocity magnitudes for the 606G_300Q_608T configuration had maximum values of 14.6 ft/s at the crest lip, illustrated in the contour map in Figure 26. Figure 27 depicts velocity contours for the 604.52G_400Q_608T configuration with maximum velocities at the crest lip of 14.5 ft/s. For the 340-bay transition, configuration 606G_260Q_608T was evaluated as displayed in Figure 28 with velocities of 13.75 ft/s at the crest lip. Similar to the 260-ft transition, the 606G_300Q_608T configuration approximately represents conditions for the 340-ft transition, which was shown to be effective in Figure 26. Velocities exceeding burst criteria of 13.1 ft/s at the crest lip are anticipated to block upstream access to sea lampreys approaching from the relatively slower flows beneath the impinging jet. Further, velocity magnitudes of 13.1 ft/s were modeled to extend fully to the free surface. For the 260-ft and 340-ft transitional operations, velocities exceeding burst criteria were noted to extend from the crest lip to the free surface and are expected to serve as an effective barrier. Velocities from the verification simulations were on the same order as the predicted velocities as a function of head loss.

Lowering of additional 20 ft of the AHS to the 360-ft bay configuration occurs at flood flows of 19,000 ft^3/s with relatively high tailwater elevations approaching 609 ft. When fully lowered, the 20-ft section relies on maintaining a sustained 8.1 ft/s over 10 ft of channel; velocities from the two-dimensional model did not exceed 13.1 ft/s. Velocities exceeding burst threshold criteria at the crest lip were the primary blockage hydraulic for the 260-ft and 340-ft transition configurations, which were not achieved for the 360-ft transition configuration. Figure 29 and Figure 30 illustrate velocities for representative 608G_120Q_608.77T and 604.52G_420Q_608.86T configurations for the 360-ft transition configuration, respectively. Velocities of 8.1 ft/s are sustained in the upper water column for over 10 ft; however, reduced velocities in the lower water column do not meet blockage design constraints. Sea lamprey may pass below the 8.1 ft/s sustained zone and attempt to pass the gate lip where velocities do not exceed burst speed requirements. Figure 31 illustrates the 360-ft transition at a point when the gate is fully lowered, at configuration 603.25G_520Q_608.9T where 8.1 ft/s or higher is sustained for 23.6 ft of channel distance which validates results from the two-dimensional model at the 360-ft configuration.

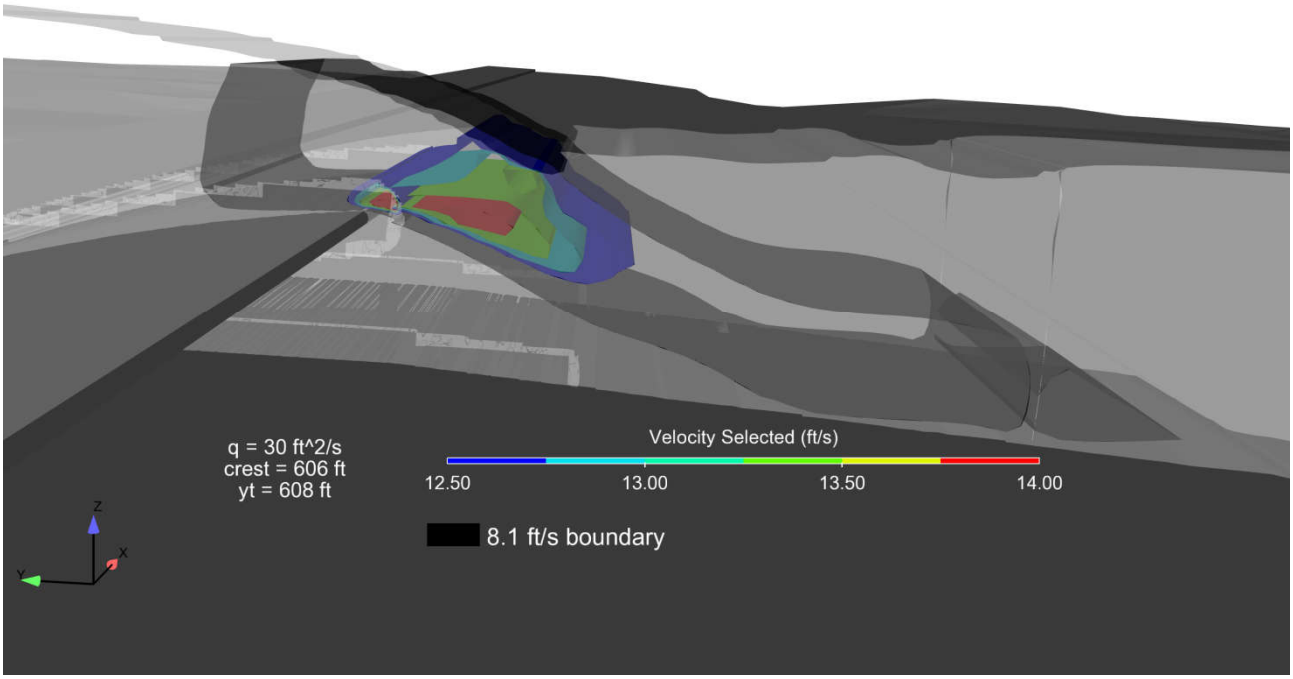

Figure 26. 606G_300Q_608T velocity contours

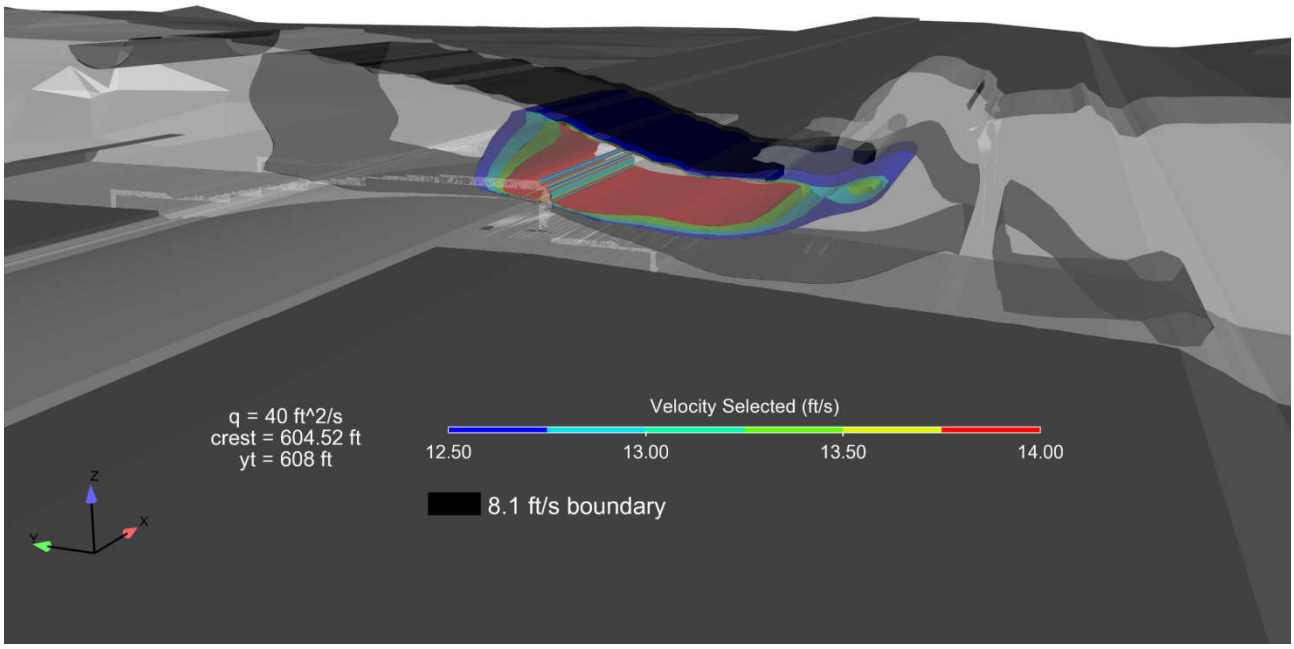

Figure 27. 604.52G_400Q_608T velocity contours

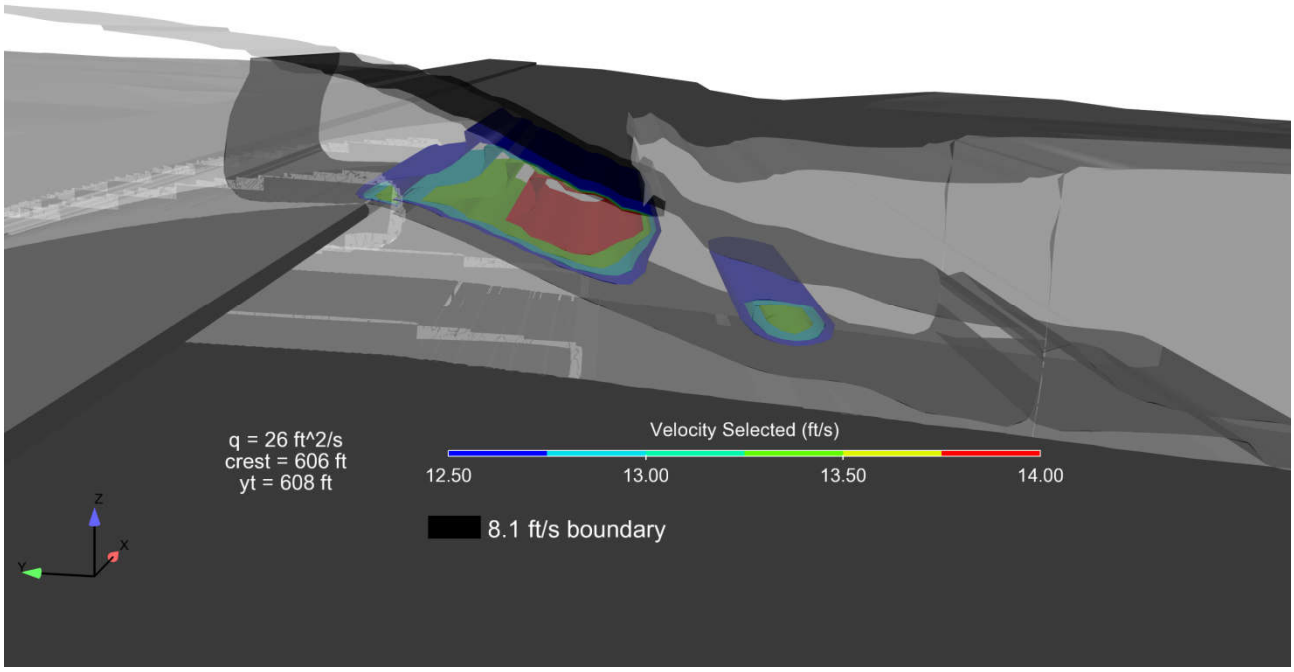

Figure 28. 606G_260Q_608T velocity contours

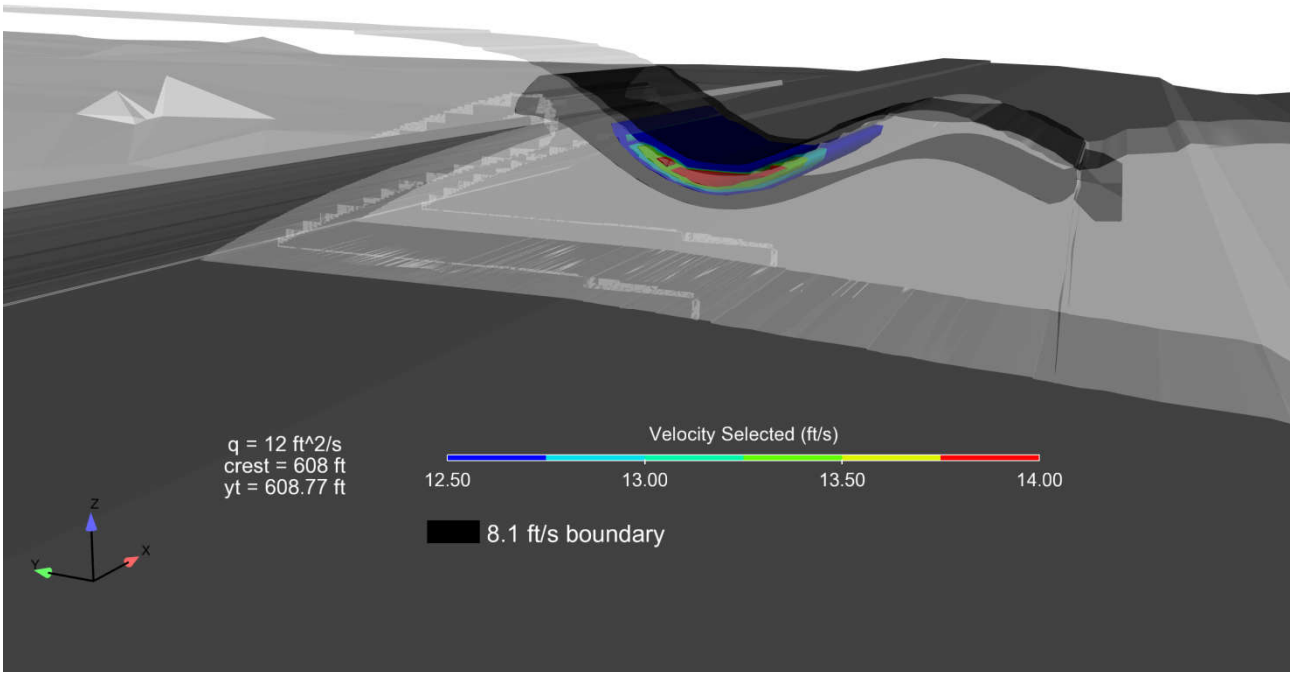

Figure 29. 608G_120Q_608.77T velocity contours

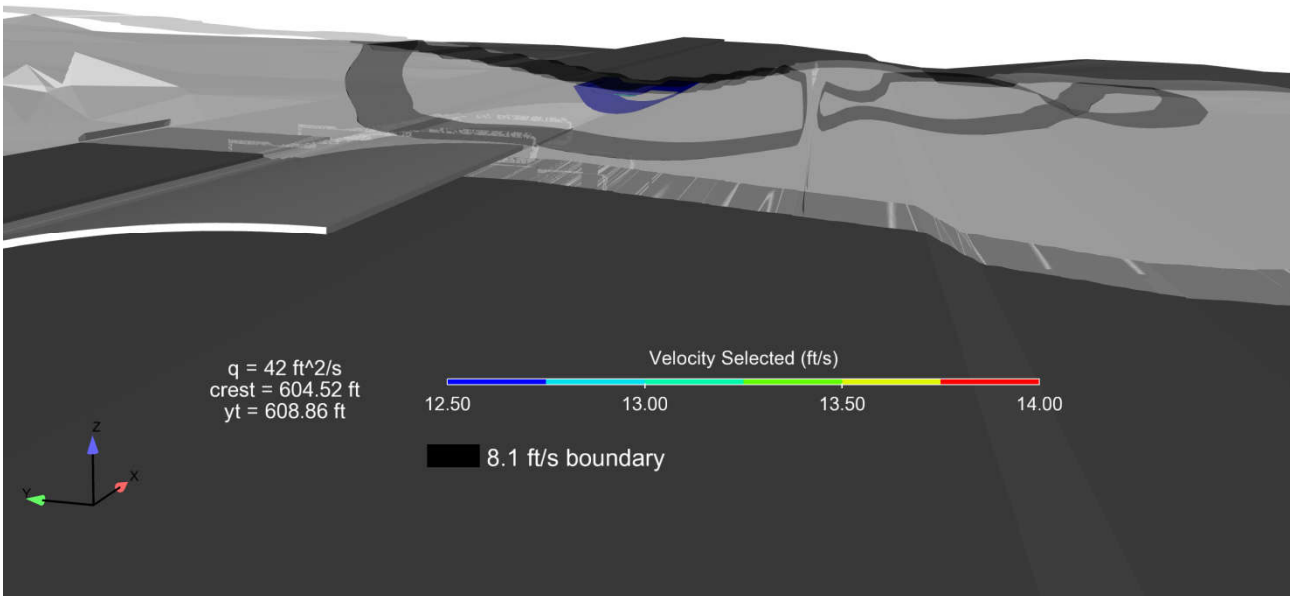

Figure 30. 604.52G_420Q_608.86T velocity contours

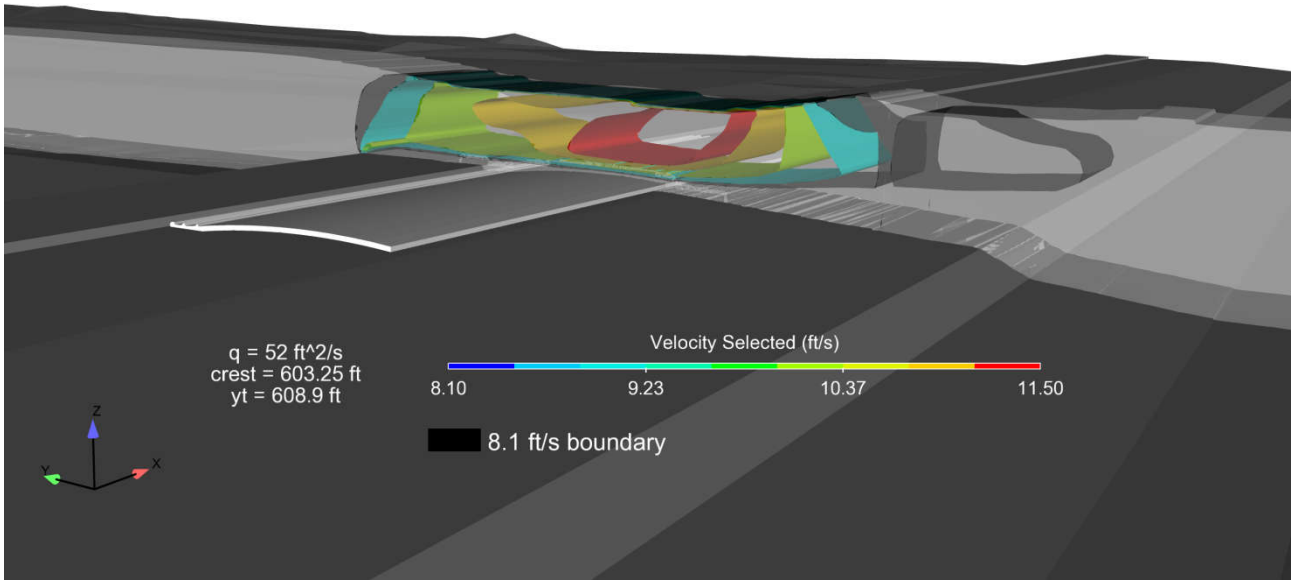

Figure 31. 603.25G_520Q_608.9T velocity contours

Results of the overtopping gate simulations also provided a measurement of the local depression in the water surface due to the interaction of the overtopping jet and tailwater. Elevations at the trough bottom typically were on the order of two feet below the tailwater at unsubmerged flows. For the 10,000 ft^3/s configuration, the water-surface elevation below the gate crest and under the jet was modeled at 605.3 ft, producing a free-overfall of 2.4 ft. The crest elevation was calculated at 1.2 ft below the tailwater elevation at that flow rate. Maintaining a free-overfall operation may be desirable for higher flow rates instead of transitioning to partial-crest configurations based on the local depression. An operational scenario where this type of management may be desired would align with a design storm that produces flow rates within the channel that fluctuate between 10,000 ft^3/s and 12,000 ft^3/s.

4.4 Hydraulic modeling summary

Detailed hydraulic modeling was performed on the AHS to determine overall operational ranges, specific structural layout, and the velocity and free-overfall hydraulic performance of the dynamically operated structure. Multi-dimensional modeling techniques were used for the varying goals. One-dimensional modeling resulted in the AHS location selection, sill and ramp design, operational ranges, and comparisons to existing conditions. Two-dimensional modeling focused the structural design to an efficient velocity barrier, identifying a geometry and layout that smoothly transitions flow through isolated channels with guide-wall structures. Simulations were used to develop rating curves to find operational limits for the partial-crest configurations, to design the gate layouts and sequencing to achieve desired hydraulics, and to verify velocity performance at break points in operations. Three-dimensional modeling was used to investigate transitional operations where gates are partially raised or lowered and the magnitude and direction of the overtopping jet velocities.

Figure 32 provides the recommended operation for the AHS with existing and proposed water surface elevations at the design constraint location at North Park. Modeling results indicated that during complete crest operations, both free-overfall and velocity criteria are surpassed and the AHS serves as an effective barrier. During partial-crest operations velocity criteria were shown to be met through dynamic operations. When gates are fully lowered, velocities through the AHS meet sustained velocity criteria throughout the full operational range (< 34,500 ft^3/s) and burst velocity criteria for flows up to approximately 19,000 ft^3/s.

Transitional gate configurations maintained burst velocity criteria at the lip of the gates for the 260-ft and 340-ft configurations. As a result of higher tailwater, the 360-ft transitional configuration was not observed to generate velocities exceeding 13.1 ft/s at the lip; therefore, a swim path exists traveling below the gate in relatively lower velocities and over the lip through velocity magnitudes of approximately 10 ft/s. Overall, the AHS was shown to meet or exceed hydraulic sea lamprey blockage criteria for the full operational range of flows up to the 20-yr flood event (34,500 ft^3/s) with the only exception being the transitional lowering of AHS-1 at approximately 19,000 ft^3/s. Design of the structural layout of the AHS, with corresponding operation for sea lamprey blockage, provides the most effective solution for achieving hydraulic blockage criteria within the project reach.

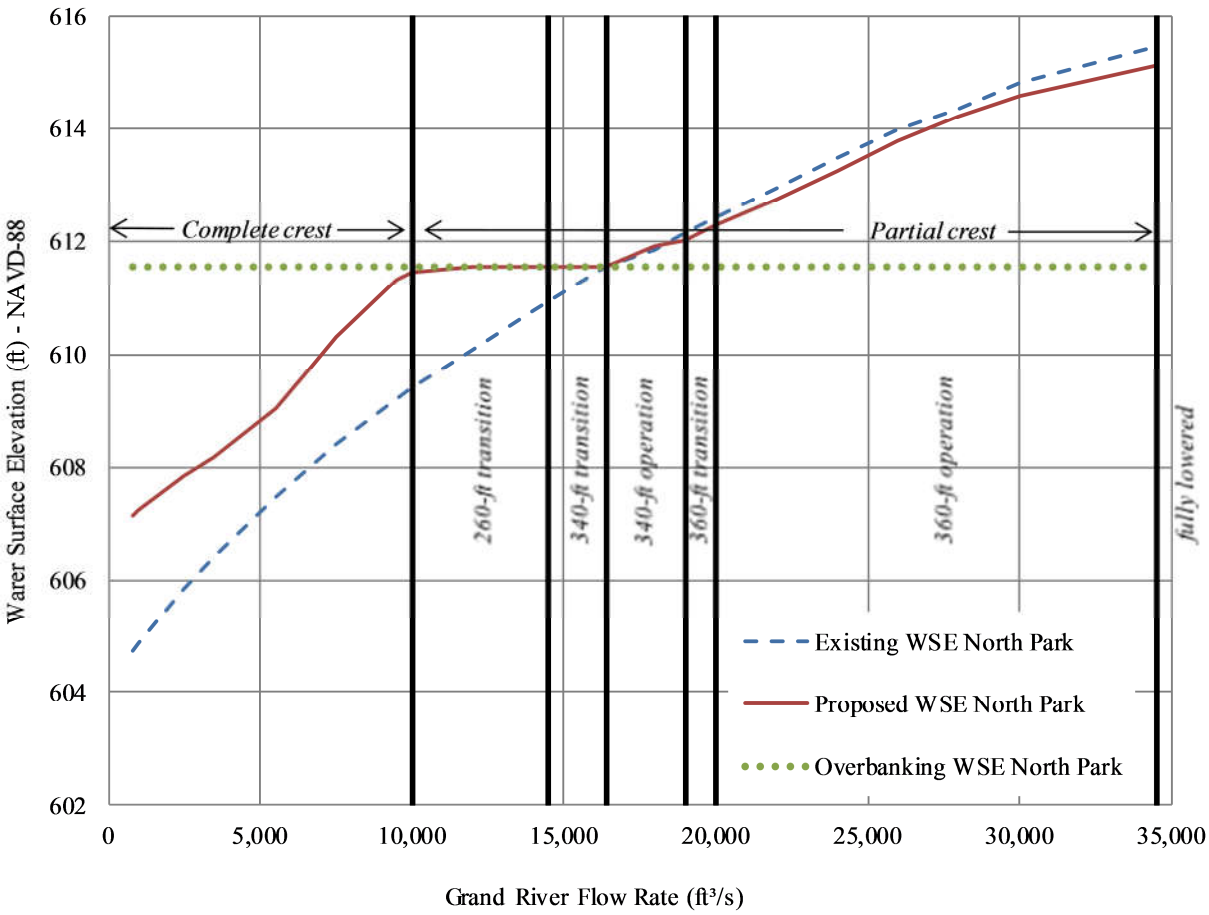

Figure 32. Recommended operations and water surfaces for the AHS

6. BOUNDARY LAYER EFFECTS

Fluid flow near surfaces transitions from a no-slip, zero velocity condition at the fluid-surface interface to the freestream velocity in the upper water column through a boundary layer. The boundary layer thickness, δ, is defined as the region where the velocity, u, is less than $0.99u_\infty$, or the free-stream velocity. In open-channel, fully turbulent flows, velocity gradients within the boundary layer are dependent upon the viscosity of the fluid, roughness of the boundary, and distance from the surface. Very close to the surface, viscous forces

within the fluid overcome inertial forces and the flow state is laminar. As distance from the surface increases, inertial forces overcome viscosity and the flow transitions to turbulent. Schlichting (1960), Pope (2000), and Wilcox (2007) expound turbulent boundary layer theory in detail. Regions within the flow are classified as the viscous sublayer, buffer layer, and log layer. Distributions of the velocity in the vertical water column follow guidelines according to the dimensionless parameters $u^+ = u/u_\tau$, where u = velocity and u_τ = shear velocity and $y^+ = u_\tau y/\nu$, where y = distance from the surface and ν = kinematic viscosity. In the viscous sublayer, $u^+ = y^+$, which has been experimentally shown to be valid for values of $y^+ < 7$. For values of $y^+ > 30$, the velocity follows a logarithmic profile of the form $u^+ = 1/\kappa \ln y^+ + C$, where $\kappa = 0.41$ and C is a constant dependent upon the roughness of the surface. For completely rough surfaces, Schlichting and Gersten (2000) found that $C \rightarrow 8.0 - 1/\kappa \ln u_\tau k_s \nu^{-1}$,where k_s = roughness height. Values of $7< y^+ < 30$ correspond to a transitional region known as the buffer layer where the function of u^+ and y^+ is ill-defined.

Verification that the boundary layer does not present a significant concern for sea lamprey passage utilized a coupled approach of numerical modeling and boundary layer theory. A section of lowered gate at 16,400 ft^3/s at the 340-ft lowered configuration was numerically simulated in three dimensions to evaluate vertical velocity profiles. The evaluated configuration produced a minimal loss in piezometric head through the structure, shown to be directly related to velocity magnitudes, and provided a conservative and representative evaluation of boundary effects. Cumulative flow through the AHS-5 gate was extracted from two-dimensional modeling and the bay was isolated for three-dimensional numerical simulation. The solution domain established a grid resolution of 1 ft, 1ft, 0.5 ft in the x, y, z directions to within one vertical foot of the AHS surface. Within the one-vertical foot region, grid resolution was set at 1 ft, 1 ft, 0.042 ft to fully resolve vertical velocity distributions near the boundary. Grid independence was shown by reducing the resolution by a factor of six near the boundary and evaluating effects in the upper water column, with a percent difference of less than 5% of the velocity magnitude. Figure 33 illustrates the steady-state solution velocity field for the evaluated configuration with streamlines indicating the smooth flow transition through AHS-5. Vertical velocity profiles were extracted within the central channel flow over the top of the gate as illustrated in Figure 34. Following the logarithmic distribution mathematical model of the flow, the vertical velocity distribution was plotted with the logarithms of the boundary distance and a best-fit linear regression line was calculated through the resulting distribution. The slope of the regression function, m, is equivalent to u_τ/κ, such that u_τ was calculated as 0.66 ft/s. Assuming a water temperature of 10°C, where sea lampreys begin spring spawning (McAuley, 1996), and with corresponding $\nu = 1.41 \times 10^{-5}$ ft/s, the viscous sublayer thickness ($y^+ < 7$) was calculated as terminating within 1.4×10^{-5} ft of the surface. The logarithmic zone of flow ($y^+ > 30$) was calculated to begin at 5.99×10^{-5} ft from the surface. Results emphasize that the zone of laminar flow, where viscosity governs flow behavior, is negligible for open-channel flow applications.

Values of k_s (in metric units) are related to Manning roughness coefficients as described by the Swamee-Jain equation, presented as Equation 3.

$$k_s \quad 3.72067 D_h e^{\left(\frac{-1.03252 D_h^{1/6}}{n}\right)} \qquad (3)$$

where:
D_h = hydraulic diameter (= 4 R, where R = hydraulic radius); and
n = Manning roughness coefficient.

Values of n for the smooth concrete and metal materials of the AHS are approximately 0.013 to 0.014 (Chow, 1959). Using the flow depth for the evaluated configuration of approximately 5 ft and n of 0.0135, the value of k_s was calculated with Equation 3 as 0.002 ft, which was assigned to the surfaces in the numerical model. Theoretical logarithmic boundary velocity profiles were calculated using the value of u_τ taken from the numerical velocity profiles, assumed k_s, and the relationships described above from

Schlichting and Gersten (2000). Values of k_s were iterated until the theoretical solution closely matched the numerical solution. The theoretical value of k_s was determined as 0.003ft, which is very close to the numerical roughness value from Equation 3 and serves to validate the numerical model ability to correctly resolve the boundary layer. Figure 36 illustrates the theoretical and numerical vertical velocity profiles as a function of boundary distance. The theoretical and numerical results deviate at approximately 0.6 ft, the approximate value of δ. Sustained velocity criteria are achieved within a nominal distance from the surface and burst velocity criteria are met within 0.35 ft of the surface. McAuley (1996) reported that sea lampreys preferentially swim approximately 0.11 ft (3.5 cm) from the surface of the channel. Sustained velocity criteria were achieved within the preferred swimming zone.

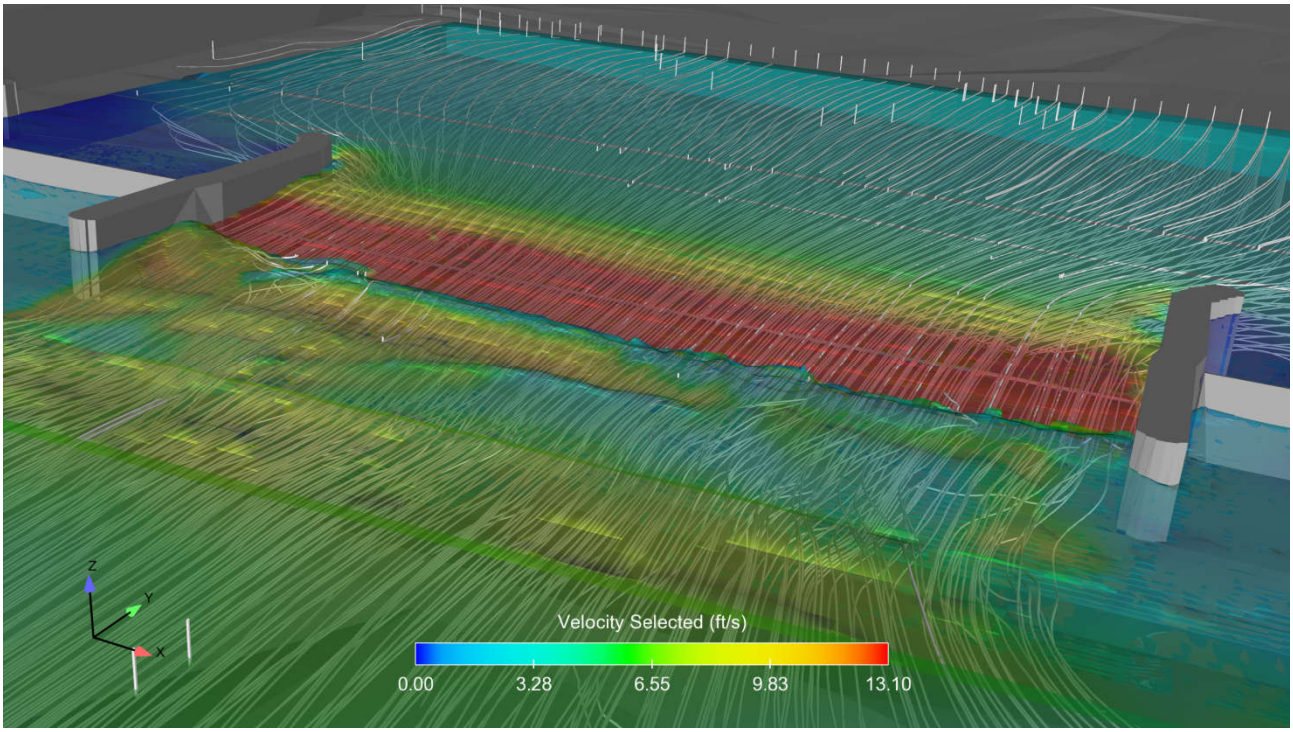

Figure 33. 16,400 ft^3/s channel flow through AHS-5; velocity magnitude and streamlines

Given the verification of the three-dimensional model to match theoretical boundary layer distributions, vertical velocity profiles were extracted at the interface between the guidewall and AHS sill as a worst-case scenario for reduced velocity at the boundary. Velocities at the interface are lower than near the channel center due to the lateral transition into the bay and the compounded boundary effects from both the sill and wall. Figure 37 illustrates the vertical velocity distributions along a transect adjacent to the guidewall and Figure 38 provides the planimetric distribution at 603.30 ft, approximately 0.05 ft above the surface. The vertical velocity distribution is provided in Figure 39. Velocities exceed the sustained velocity threshold at a negligible distance from the surface and the burst velocity criteria within 0.35 ft of the surface.

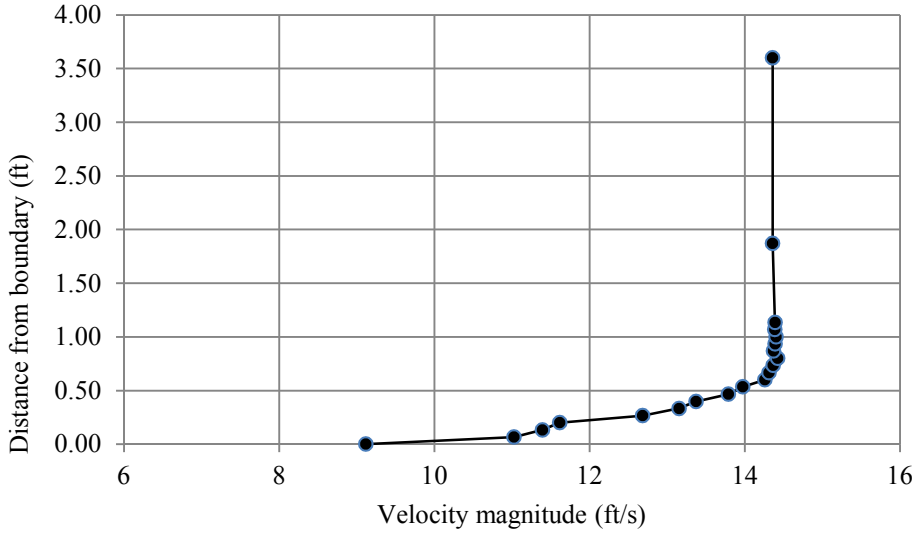

Figure 34. Representative vertical velocity profile from channel center; 16,400 ft^3/s – 340 ft-configuration

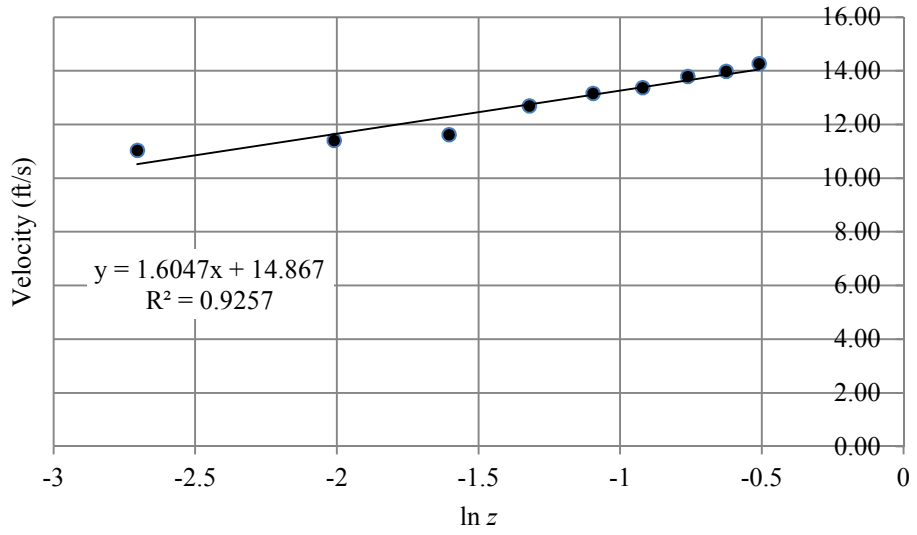

Figure 35. Velocity magnitude distribution as a function of ln(z); 16,400 ft^3/s – 340 ft-configuration

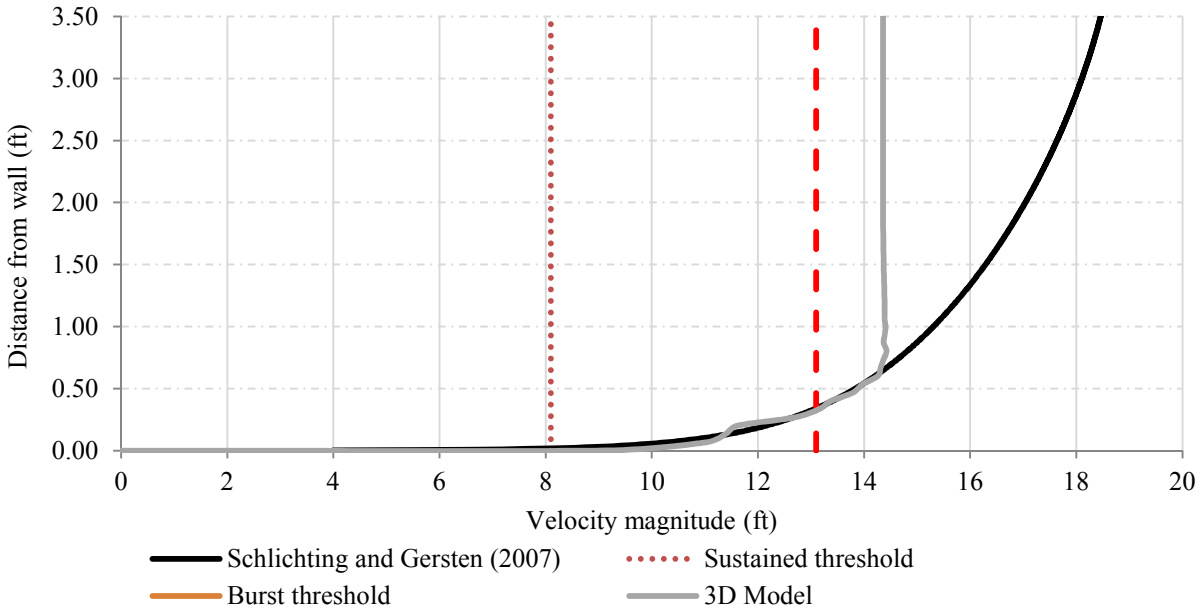

Figure 36. Theoretical and modeled velocity profiles over the AHS crest; 16,400 ft^3/s – 340 ft-configuration

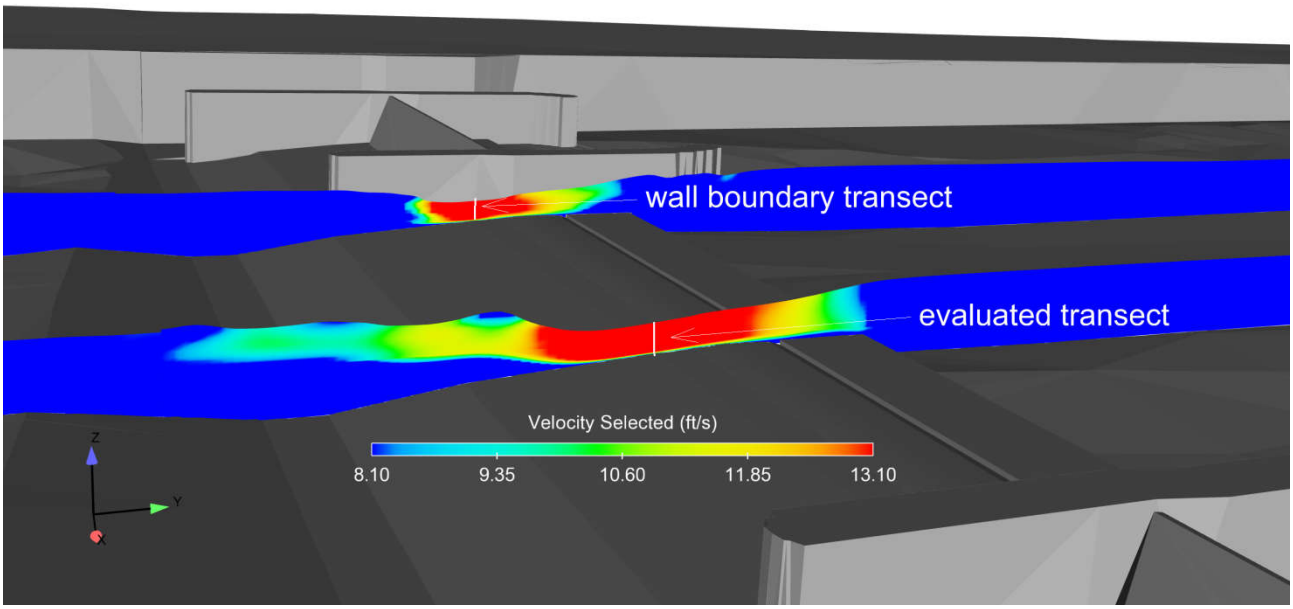

Figure 37. Velocity magnitude for evaluated configuration at longitudinal transects; 16,400 ft^3/s – 340 ft-configuration

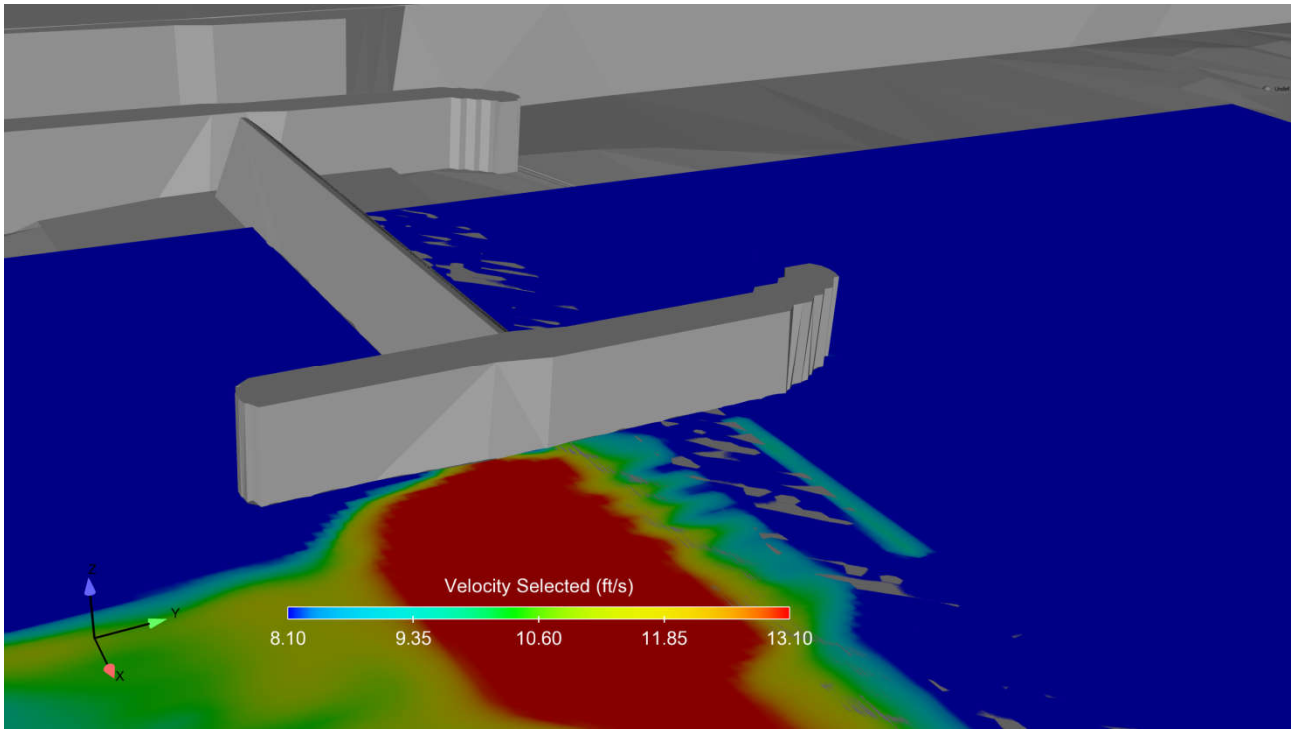

Figure 38. Velocity magnitude at elevation 603.30 ft, 0.05 ft off boundary; 16,400 ft^3/s – 340 ft-configuration

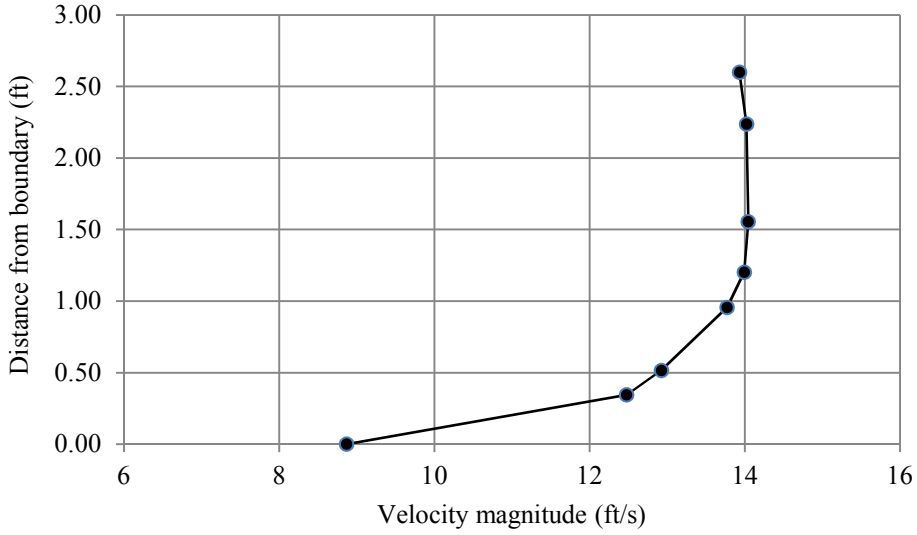

Figure 39. Vertical velocity distribution near wall boundary at 16,400 ft^3/s 340-ft configuration

7. DISCUSSION

The design of the AHS achieves two separate hydraulic blockage criteria by incorporating dynamic

operational capabilities with a tailored structural geometry. This unique layout allows for the operation of the structure at a much larger range of flows than for a structure that just provides free-overfall or velocity blockage. Static free-overfall structures are limited by upstream overbanking and cannot maintain a barrier when the tailwater rises above the designed crest height. Similarly, velocity barrier structures which typically resemble broad-crested weirs or chutes lose function at lower flows when supercritical velocities are too slow or at higher flows when the tailwater submerges the supercritical transition. The multi-criteria design of the AHS exceeds performance of traditional barriers and has many positive implications for future barrier construction in the Great Lakes Fishery. This type of design is scalable and readily applied to various stream sizes and design constraints.

The barrier is most effective in both complete-crest or partial-crest operations at lower flows, primarily as a function of the relatively lower tailwater compared to the AHS crest and sill elevations and increased head differences. Flow rates of high effectiveness correspond to sea lamprey spawning periods, typically between May and early July where water temperatures are high. The hydrology and temperature of the Grand River related to sea lamprey spawning migration is further detailed in RiverRestoration (2016b). When flows within the channel are on the order of magnitude of 16,400 ft^3/s or greater at peak discharges typically during late March to early April, the water temperature is approximately 5°C to 10°C where sea lamprey mobility is significantly impaired.

Operational recommendations for the AHS provide fully developed hydraulics across the guided channel bays. The AHS was designed to be self-maintaining by producing boundary shear stresses which mobilize incoming sediment loads in suspension through the structure. No sediment accumulation is expected on the upstream side of the gates during partial-crest operations which may affect hydraulic performance. However, the potential for disrupted hydraulic fields was considered during design. Large woody debris, vandalism, mechanical failure, or unforeseen events may create hydraulic conditions which do not meet criteria and necessitate maintenance to the AHS. Unanticipated hydraulic conditions may be addressed with the inclusion of electrical systems which deter upstream sea lamprey migration (Smith and Root, 2012). At minimum, AHS-1 will be fitted with an electrical barrier system to address the transitional period between the 340-ft and 360-ft operations, which is the only anticipated point where electricity is not designed as a fail-safe addition.

Swimming performance criteria from the literature served as the primary guidelines for the design of the AHS. A secondary objective of the design was to meet the same level of blockage as the existing 6th Street Dam. RiverRestoration (2016a) details a one-dimensional feasibility of the proposed conditions compared to the existing conditions pertaining to sea lamprey hydraulics. At the only point during operation where hydraulic criteria are not achieved at the AHS, the existing 6th Street Dam is submerged and has flow paths that are able to be exploited by migrating sea lamprey. The proposed AHS meets the performance of the 6th Street Dam across the full hydrograph.

Operation of the AHS in any application must assume an upstream overbanking design constraint. For the application to the Grand River, the constraint location was set at North Park with a overbanking water surface elevation of 611.53 ft, corresponding to 16,400 ft^3/s. Inherent variability in gage data, discharge measurements, and modeling assumptions may dictate that the overbanking elevation be field-fitted to a more accurate value. In such a case, the overall operational structure of the AHS will not change; however, the exact flow rates at which transitions occur may shift slightly. Fully lowered partial-crest configurations were shown to be effective at the flow rate at which the transition started (e.g. 10,000 ft^3/s at the 260-ft configuration). Results provide confidence that hydraulic design criteria will be met in case the adjusted operation shifts towards reduced upstream head and lowered discharges.

8. CONCLUSION

An adjustable hydraulic structure was proposed for construction within the Grand River at Grand Rapids, MI as part of the Grand Rapids Revitalization Project. The main purpose of the AHS is to achieve hydraulic performance criteria shown in the literature to block upstream passage of sea lampreys. Multi-dimensional hydraulic modeling was conducted for the innovation of a new barrier design which functionally meets hydraulic design criteria while achieving upstream overbanking constraints. The AHS dynamically meets both free-overfall and velocity blockage hydraulics which allows operation at a larger range of flows than for a statically operated structure. The structural layout and operational recommendations are an improvement on traditional barrier designs and may be readily implemented in other rivers where sea lamprey migration is a concern.

9. REFERENCES

Anderson, D., Moggridge, H., Warren, P., and Shucksmith, J. (2014). "The impacts of 'run-of-river' hydropower on the physical and ecological condition of rivers." *Water and Environmental Journal* 29(2): 268-276

Beamish, F.W.H. (1974). "Swimming performance of adult sea lamprey, (*Petromyzon marinus*), in relation to weight and temperature." *Trans. Am. Fish. Sco.* 103:355-358.

Chow, V.T. (1959). *Open-channel Hydraulics*. McGraw Hill. New York, NY.

Fishbeck ,Thompson, Carr & Huber (2010). HEC-RAS Effective Model, Grand River.

FlowScience (2016). "Flow-3D v11.1.0 user manual." FlowScience, Inc.

Gordon, E.H., Collins, K., Holmquist-Johnson, C., and S.M. Scurlock (2016). "Rock weir design guidance." U.S. Department of the Interior Bureau of Reclamation Technical Service Center. Denver, CO.

Great Lakes Fishery Commission (2000). "Sea lamprey – A Great Lakes invader." GLFC. www.seagrant.umn.edu/downloads/x106.pdf. Accessed Feb, 2016.

Great Lakes Fishery Commission (2016). "Sea lamprey barriers – limiting sea lamprey access to spawning habitat." GLFC. www.glfc.org/pubs/FACT_5.pdf. Accessed Feb, 2016.

Hanson, L.H. (1980). "1980 Study to determine the burst swimming speed of spawning-run sea lampreys (*Petromyzon marinus*)." *Research Completion Report,* U.S. F.W.S. Millerburg, Michigan

Hanshue, S.K & Harrington, A.H. (2011). Special Report Draft Grand River Assessment Michigan Department of Natural Resources Fisheries Division.

Hunn, J.B., and W.D. Youngs. (1980). Role of Physical Barriers in the Control of Sea Lamprey *(Petromyzon marinus)*. Can. J. Fish. Aquat. Sci. 37: 2118-2122.

McAuley, Thomas C. (1996). Development of an instream velocity barrier to stop sea lamprey (*Petromyzon Marinus*) migrations in Great Lakes Streams. Master of Science Thesis. Department of Civil engineering, at the University of Manitoba. Winnipeg, Manitoba. April, 1996.

National Oceanic and Atmospheric Agency (2016). "Grand River at Grand Rapids." http://water.weather.gov/ahps2/hydrograph.php?wfo=grr&gage=gdrm4. Last accessed April, 2016.

Obermeyer, Inc. (2016). "Discharge Performance." Obermeyer, Inc. *in draft*.

Pope, S.B. (2000). *Turbulent Flows*. Cambridge Press. New York, NY.

Rantz, S.E. (1982). "Measurement and computation of streamflow: Volume 1. Measuremen of stage and discharge." *Geological Survey Water-supply paper 2175.* USGS.

RiverRestoration (2016a). "Adjustable hydraulic structure feasibility for restricted passage of sea lamprey (*Petromyzon marinus*)." *Grand Rapids Revitalization Report* – Appendix J. *in draft*.

RiverRestoration (2016b). "Grand River Hydrology." *Grand Rapids Revitalization Report* – Appendix H. *in draft*.

RiverRestoration (2016c). "Fish passage over a dam or barrier." *Grand Rapids Revitalization Report* – Appendix K. *in draft*.

Schlichting, H. (1960). *Boundary Layer Theory*. McGraw Hill. New York, NY.

Schlichting H. and Gersten, K. (2000). *Boundary Layer Theory,* Eighth Ed. Springer-Verlag, Berlin, Germany.

United States Bureau of Reclamation (2008). "SRH-2D: Theory and user Manual." U.S. Department of the Interior Bureau of Reclamation Technical Service Center. Denver, CO.

USACE, 2016. HEC-RAS River Analysis System Hydraulic Reference Manual version 5. http://www.hec.usace.army.mil/software/hec-ras/documents/HEC-RAS_5.0_Reference_Manual.pdf . U.S. Army Corps of Engineers Hydrologic Engineering Center. Davis, CA.

Wilcox, D.C. (2007). *Basic Fluid Mechanics*. DCW Industries.